



HAL
open science

Koopman–Hill stability computation of periodic orbits in polynomial dynamical systems using a real-valued quadratic harmonic balance formulation

Fabia Bayer, Remco I. Leine, Olivier Thomas, Aurélien Grolet

► To cite this version:

Fabia Bayer, Remco I. Leine, Olivier Thomas, Aurélien Grolet. Koopman–Hill stability computation of periodic orbits in polynomial dynamical systems using a real-valued quadratic harmonic balance formulation. *International Journal of Non-Linear Mechanics*, 2024, 167, pp.104894. 10.1016/j.ijnonlinmec.2024.104894 . hal-04721112

HAL Id: hal-04721112

<https://hal.science/hal-04721112v1>

Submitted on 4 Oct 2024

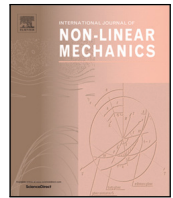
HAL is a multi-disciplinary open access archive for the deposit and dissemination of scientific research documents, whether they are published or not. The documents may come from teaching and research institutions in France or abroad, or from public or private research centers.

L'archive ouverte pluridisciplinaire **HAL**, est destinée au dépôt et à la diffusion de documents scientifiques de niveau recherche, publiés ou non, émanant des établissements d'enseignement et de recherche français ou étrangers, des laboratoires publics ou privés.



Contents lists available at ScienceDirect

International Journal of Non-Linear Mechanics

journal homepage: www.elsevier.com/locate/nlm

Koopman–Hill stability computation of periodic orbits in polynomial dynamical systems using a real-valued quadratic harmonic balance formulation

Fabia Bayer^{a,*}, Remco I. Leine^a, Olivier Thomas^b, Aurélien Grolet^b

^a University of Stuttgart, Pfaffenwaldring 9, 70569 Stuttgart, Germany

^b Arts et Métiers Institute of Technology, LISPEN, 59000 Lille, France

ARTICLE INFO

Keywords:

Floquet multipliers

Path-following

Frequency response function

Hill's determinant

Quadratic recast

Monodromy matrix

ABSTRACT

In this paper, we generalize the Koopman–Hill projection method, which was recently introduced for the numerical stability analysis of periodic solutions, to be included immediately in classical real-valued harmonic balance (HBM) formulations. We incorporate it into the Asymptotic Numerical Method (ANM) continuation framework, providing a numerically efficient stability analysis tool for frequency response curves obtained through HBM. The Hill matrix, which carries stability information and follows as a by-product of the HBM solution procedure, is often computationally challenging to analyze with traditional methods. To address this issue, we generalize the Koopman–Hill projection stability method, which extracts the monodromy matrix from the Hill matrix using a matrix exponential, from complex-valued to real-valued formulations. In addition, we propose a differential recast procedure, which makes this real-valued Hill matrix immediately available within the ANM continuation framework. Using as an example a nonlinear von Kármán beam, we demonstrate that these modifications improve computational efficiency in the stability analysis of frequency response curves.

1. Introduction

The harmonic balance Method (HBM) serves as a valuable instrument in the analysis of nonlinear dynamical systems subject to periodic forcing. It is employed in wide ranges of engineering applications including turbomachinery [1], geared systems [2], acoustics [3] and structural dynamics [4]. Typically, HBM is employed within a path-following, often also called continuation, framework to find branches of periodic solutions along a varying parameter. With the aim to understand and usually mitigate vibrations in engineering applications, this tool is employed to generate nonlinear frequency response curves, i.e., compute the nonlinear periodic response of a forced system across a range of excitation frequencies, or compute the nonlinear free conservative response to obtain the nonlinear modes of the system in the form of their backbone curves and deformed shapes [4].

The state-of-the-art methods for the numerical stability analysis of periodic solutions can be categorized into two families, as their corresponding operations take place either in the time or the frequency domain [5,6]. Time domain methods determine the monodromy matrix by numerical integration of a linear matrix differential equation of the size of the original problem over one period. Employed in HBM settings,

these methods do not take advantage of the frequency nature of the HBM and require reverting back to time domain exclusively for stability determination. In contrast, frequency domain methods, also commonly called Hill methods, are based on the Hill matrix, which is strongly related to the Jacobian of the HBM residual. Some of the eigenvalues of this matrix approximate the Floquet exponents, which allow to assess the stability. So-called *sorting methods* select an appropriate subset of the complete eigenspectrum. These sorting methods are based on the eigenvalues themselves [7,8] or the eigenvectors [9,10]. Classically, the Hill matrix is presented in a complex-valued form that exhibits a banded block-Toeplitz structure, but in application it is often obtained in a more practical real-valued formulation that has an identical set of eigenvalues [11]. Recently, the authors proposed the Koopman–Hill projection stability method that combines time-domain and frequency-domain aspects as it determines the monodromy matrix from the classical complex-valued formulation of the Hill matrix using a matrix exponential and a projection [12,13].

One specific continuation framework is the Asymptotic Numerical Method (ANM). Coupled to the HBM, the ANM computes continuous solution branches of first order differential algebraic systems with

* Corresponding author.

E-mail addresses: bayer@inm.uni-stuttgart.de (F. Bayer), leine@inm.uni-stuttgart.de (R.I. Leine), Olivier.THOMAS@ensam.eu (O. Thomas), Aurelien.GROLET@ensam.eu (A. Grolet).

<https://doi.org/10.1016/j.ijnonlinmec.2024.104894>

Received 22 April 2024; Received in revised form 28 August 2024; Accepted 2 September 2024

Available online 10 September 2024

0020-7462/© 2024 The Author(s). Published by Elsevier Ltd. This is an open access article under the CC BY license (<http://creativecommons.org/licenses/by/4.0/>).

purely quadratic polynomial nonlinearities [9,14]. A large class of dynamical systems involving smooth nonlinearities, such as polynomials of arbitrary degree, rational functions, or regularized friction, can be recast into this form [15–17]. In this case, the computation of the real-valued Hill matrix is straightforward using a condensation operation, leading to a rather efficient method for stability computation that can be executed fully in the frequency domain [9].

Despite its prevalence across engineering domains and irrespective of the continuation framework employed, there are persistent challenges in the state-of-the-art numerical stability analysis of periodic solutions found by HBM, mainly because of the computational cost. For large-scale systems, the numerical integrations needed to obtain the monodromy matrix in the time domain are often more costly than finding the periodic solution itself [18–20]. In the frequency domain, the solution of the complete eigenvalue problem is also a very costly operation [6], hampering the use of sorting methods. Therefore, stability computation constitutes a bottleneck during the continuation procedure. The overarching aim of the present work is to address these issues by integrating the Koopman–Hill projection stability method, which requires neither numerical integration nor the solution of the complete eigenproblem and can be more efficient than sorting methods [12], into the ANM continuation framework.

Two central challenges complicate the immediate application of the Koopman–Hill method in the ANM. Firstly, we show that the condensation operation that relates the HBM equations to the Hill matrix for the differential algebraic equation systems (DAE) resulting from the classical quadratic recast induces truncation errors, which impact the accuracy of the Koopman–Hill projection approach more than that of the classical sorting-based approaches. To remedy this, we introduce in Section 3 a differential recasting procedure that arrives at a quadratic ordinary differential equation instead of a DAE, such that the Hill matrix is available immediately without the need for a condensation operation. A second challenge is posed by the fact that the Koopman–Hill projection has until now only been derived for the classical complex-valued Hill matrix, but the ANM framework (with or without the condensation) returns the Hill matrix in its real-valued form. In Section 4, we explicitly derive the problem-independent similarity transforms relating any two Hill matrix formulations and use these to generalize the Koopman–Hill projection method to arbitrary Fourier bases. This generalization is applicable to any Hill problem independent of how the Hill matrix is obtained, but in particular also for the Hill matrix given in ANM. Finally, in Section 5, we illustrate the effectiveness of the Koopman–Hill projection method coupled to ANM with a differential recast, using a modal reduction of a periodically forced von Kármán beam as an example of arbitrary size with polynomial nonlinearities.

2. Theoretical background

In this section, we provide some theoretical background on the methods used in this work, with a particular focus on frequency-based continuation methods for finding periodic solutions and determining their stability.

2.1. Harmonic balance method

Consider a finite-dimensional dynamical system governed by

$$\dot{\mathbf{x}} = \mathbf{f}(\mathbf{x}, t), \quad (1)$$

where $t \in \mathbb{R}$ denotes time, $\mathbf{x}(t) \in \mathbb{R}^n$ lies on a state trajectory initialized at $\mathbf{x}(0) = \mathbf{x}_0$ and $\mathbf{f} : \mathbb{R}^n \times \mathbb{R} \rightarrow \mathbb{R}^n$ is a sufficiently smooth vector field which is T -periodic in t .

A T -periodic solution is a solution \mathbf{x}^p of (1) which fulfills $\mathbf{x}^p(t+T) = \mathbf{x}^p(t)$ for all $t \geq 0$. The problem of finding such solutions is a boundary value problem (BVP) as conditions are imposed on both initial and terminal state. Various methods exist to address this type of BVP, both

in the time domain and in the frequency domain. Techniques such as shooting, multiple shooting, and collocation all rely on an interplay between time-integration (or finite differencing) of the ordinary differential equation (ODE) (1) and solving nonlinear functions for periodicity and continuity constraints [21]. In contrast, the harmonic balance method (HBM) [5,6,10,22,23] is a frequency-based method, which aims to determine a set of Fourier coefficients approximating the periodic solution. The sought unknown periodic solution can be approximated by its complex-valued Fourier expansion up to order N via

$$\mathbf{x}^p(t) = \sum_{k=-N}^N \mathbf{x}_k e^{ik\omega t} =: \mathbf{x}^p(\mathbf{X}_{\text{cplx}}, t) \quad (2)$$

with $\omega = \frac{2\pi}{T}$ and $\mathbf{X}_{\text{cplx}} := (\mathbf{x}_{-N}^T, \dots, \mathbf{x}_N^T)^T \in \mathbb{C}^{n(2N+1)}$ gathering the corresponding unknown complex-valued coefficients in a column vector. Since the periodic solution is known to be real-valued, it can equivalently be expressed by a real-valued Fourier series

$$\mathbf{x}^p(t) = \mathbf{a}_0 + \sum_{k=1}^N \mathbf{a}_k \cos k\omega t + \mathbf{b}_k \sin k\omega t =: \mathbf{x}^p(\mathbf{X}_{\text{real}}, t) \quad (3)$$

with $\mathbf{X}_{\text{real}} := (\mathbf{a}_0^T, \dots, \mathbf{a}_N^T, \mathbf{b}_1^T, \dots, \mathbf{b}_N^T)^T \in \mathbb{R}^{n(2N+1)}$ as vector of unknowns. The arrangement of the coefficients within \mathbf{X}_{real} is an arbitrary choice that does not influence the results of the procedure, and various arrangements can be found in the literature. Given the equivalence between complex and real representations, many of the subsequent developments operate with a general vector \mathbf{X} of unknown coefficients, implicitly assuming the use of the corresponding Fourier series. In Section 4, we will illustrate linear transformations that facilitate easy switching between the formulations.

In the HBM, the unknown coefficients \mathbf{X} are determined by substituting the corresponding Fourier series into the dynamics (1) to obtain the residual in time

$$\mathbf{r}(\mathbf{X}, t) = \mathbf{f}(\mathbf{x}^p(\mathbf{X}, t), t) - \dot{\mathbf{x}}^p(\mathbf{X}, t). \quad (4)$$

The residual \mathbf{r} is then expressed as a Fourier series, and its first N harmonics are required to vanish in a Galerkin procedure. This procedure yields the $n(2N+1)$ algebraic equations

$$\mathbf{R}(\mathbf{X}) = \mathbf{0}. \quad (5)$$

Existence and convergence of these HBM approximations have been shown under suitable assumptions [5]. While the derivative component of (4) as well as linear terms in \mathbf{f} are easy to handle, the frequency decomposition of the nonlinear terms in \mathbf{f} can usually not be expressed in closed form, except if the nonlinearities are polynomials of low degree. In order to apply standard predictor–corrector methods, the individual equations for each order are thus often determined and simultaneously solved using the fast Fourier transform with an alternating frequency and time (AFT) method, evaluating \mathbf{f} in the time domain after an inverse Fourier transformation of the unknowns in each iteration step [24]. An alternative to the AFT and predictor–corrector methods is the ANM framework, for which the solution branches are computed using a higher-order Taylor series expansion, provided the nonlinear part of $\mathbf{R}(\mathbf{X})$ contains only quadratic polynomials. This method will be described in Section 2.4 in detail.

2.2. Floquet theory and stability of periodic solutions

Below we recapitulate some classical results of Floquet theory, which can be found in standard textbooks, (e.g. [18,25,26]). Consider a T -periodic orbit \mathbf{x}^p of (1). Typically, such an orbit is obtained with sufficient accuracy using methods like HBM or other periodic solution solvers. To study stability, we consider a small perturbation $\mathbf{y} := \mathbf{x} - \mathbf{x}^p$ around the periodic orbit. After linearization, the dynamics of this perturbation is governed by the perturbation equation

$$\dot{\mathbf{y}}(t) = \left. \frac{\partial \mathbf{f}(t, \mathbf{x})}{\partial \mathbf{x}} \right|_{\mathbf{x}^p(t)} \mathbf{y}(t) := \mathbf{J}(t)\mathbf{y}(t), \quad (6)$$

i.e., a linear dynamical system with a time-periodic system matrix. In the hyperbolic case, stability of the equilibrium of (6) coincides with orbital stability of the periodic solution [18].

By virtue of linearity, there exists a principal fundamental solution matrix $\Phi(t)$ of (6), which maps initial conditions at time 0 to time t , i.e.

$$\mathbf{y}(t) = \Phi(t)\mathbf{y}(0) \quad (7)$$

for all times $t \in \mathbb{R}$ and all initial conditions $\mathbf{y}(0) \in \mathbb{R}^n$ [25]. The matrix $\Phi(T) := \Phi_T$ evaluated after one period is called the monodromy matrix and its eigenvalues $\{\lambda_i\}_{i=1}^n$ are called Floquet multipliers [18]. If all eigenvalues of Φ_T lie strictly inside the unit circle, then the magnitude of any trajectory of (6) will decay over time, indicating asymptotic stability of the equilibrium. Conversely, if a Floquet multiplier has an eigenvalue strictly larger than 1, the equilibrium is unstable.

Floquet's theorem [25,27] states that the fundamental solution matrix can be expressed as the product

$$\Phi(t) = \mathbf{P}(t)e^{\mathbf{Q}t} \quad (8)$$

where $\mathbf{P}(t) = \mathbf{P}(t+T)$ is a T -periodic matrix in $\mathbb{C}^{n \times n}$ and $\mathbf{Q} \in \mathbb{C}^{n \times n}$ is a constant matrix. The eigenvalues $\alpha_1, \dots, \alpha_n$ of \mathbf{Q} are known as Floquet exponents and are related to the Floquet multipliers via

$$\lambda_i = e^{\alpha_i T}, \quad i = 1, \dots, n. \quad (9)$$

For each of the n Floquet multipliers λ_i , there exists an infinite number of Floquet exponents that fulfill (9), related to each other by $\tilde{\alpha}_i = \alpha_i + ki\frac{2\pi}{T}$ with $k \in \mathbb{Z}$. If α is a Floquet exponent, then there exists a corresponding Floquet form solution [18]

$$\mathbf{y}_\alpha(t) = \mathbf{p}_\alpha(t)e^{\alpha(t-t_0)} \quad (10)$$

of (6), where $\mathbf{p}_\alpha(t) = \mathbf{p}_\alpha(t+T) \in \mathbb{C}^n$ is a T -periodic function.¹ These Floquet form solutions can be used to compute the Lyapunov–Floquet transformation, which brings (6) into a linear time-invariant (LTI) form [25].

Hill's method, closely related to Hill's determinant method [10,18], offers a frequency-domain-based approach to approximate the Floquet exponents of (6). By explicitly evaluating the complex-valued Fourier series of an unknown Floquet form, it follows that the Floquet exponents are part of the spectrum of the infinite Hill matrix \mathbf{H}_∞ , which is composed of the complex-valued Fourier coefficients of the periodic system matrix $\mathbf{J}(t) = \sum_{k=-\infty}^{\infty} \mathbf{J}_k e^{i\omega kt}$ with blocks $\mathbf{H}_{jk} = \mathbf{J}_{j-k} - ik\omega\delta_{kj}\mathbf{I}$ for $j, k = -\infty, \dots, \infty$ [10]. Notably, in a block-Toeplitz fashion, all block entries along each sub- or superdiagonal of \mathbf{H}_∞ have the identical value $\mathbf{H}_{jk} = \mathbf{H}_{j+l, k+l} = \mathbf{H}_{j-k}$.

In practice, only the eigenvalues of a finite-dimensional matrix approximation of the infinite Hill matrix can be computed numerically. The matrix \mathbf{H} of size $n(2N+1) \times n(2N+1)$ consists of the $n(2N+1)$ most centered rows and columns of \mathbf{H}_∞ and approximates the original infinite-dimensional Hill matrix. In Section 4.1 we provide a proof of the well-known fact that the Jacobian matrix of the HBM equations coincides with the truncated Hill matrix, making this matrix immediately available in HBM settings without further construction steps. In practice, therefore, the block-by-block construction process for the Hill matrix outlined in the present section is not necessary. In particular, the Jacobian matrix was used for all numerical examples of this work.

While one might naively expect that the eigenvalues of \mathbf{H} coincide with a subset of the Floquet exponents, this is generally not the case due to truncation errors. If no additional steps are taken, spurious eigenvalues without physical meaning may lead to the assertion of instability in

¹ If \mathbf{Q} or, equivalently, Φ_T are not diagonalizable, then there exist additional Floquet form solutions of the form (10) where \mathbf{p}_α also has non-periodic polynomial components. However, for every Floquet exponent, there exists at least one Floquet form with purely periodic $\mathbf{p}_\alpha(t)$ [18]. Only this purely periodic Floquet form is required for the developments below.

stable cases, giving the method a reputation of being inaccurate [5,6]. However, this issue can be mitigated if only a subset of eigenvalues is considered for stability determination instead of all $n(2N+1)$ of them. In this case, sorting methods are required to identify those eigenvalues that are most likely to approximate all Floquet exponents well. These methods rely on symmetry considerations of the eigenvectors [9,10] or on the magnitude of the imaginary part [7,8,22,28].

For all sorting methods, there currently exist no means to efficiently and accurately compute only those eigenvalues that are sought. Instead, all eigenpairs of \mathbf{H} are computed first, and then most of them are discarded, resulting in significant computational cost [6]. Sparsity of \mathbf{H} cannot be reasonably exploited to decrease the computational cost of solving the complete eigenvalue problem [29].

2.3. Koopman–Hill projection stability method

In a recent publication by the authors [12,13], an alternative approach based on the Koopman formalism [30] has been introduced to derive the Floquet quantities from the Hill matrix. This approach does not rely on solving the complete eigenvalue problem of the Hill matrix and is therefore not bound by the computational limitations of the classical approaches of Section 2.2.

In [12], we showed that the linear time-invariant dynamical system $\dot{\mathbf{z}} = \mathbf{H}\mathbf{z}$ defined by the truncated Hill matrix of order N coincides with the linear truncated Koopman lift of (6) for a specific set Ψ of observables defined by

$$\Psi(t, \mathbf{y}(t)) := (e^{iN\omega t} \quad e^{i(N-1)\omega t} \quad \dots \quad e^{-iN\omega t})^T \otimes \mathbf{y}(t), \quad (11)$$

where \otimes denotes the Kronecker product. The entries of $\mathbf{y}(t)$ in (11) are ordered by *descending* frequency. This slightly unusual choice ensures that for any initial condition $\mathbf{y}(0)$ of $\dot{\mathbf{y}}(t) = \mathbf{J}(t)\mathbf{y}(t)$, choosing the initial condition of $\dot{\mathbf{z}} = \mathbf{H}\mathbf{z}$ in agreement with (11) as

$$\mathbf{z}(0) = \Psi(0, \mathbf{y}(0)) = (1 \quad \dots \quad 1)^T \otimes \mathbf{y}(0) =: \mathbf{W}\mathbf{y}(0) \quad (12)$$

yields the approximation

$$\mathbf{z}(t) =: (\mathbf{z}_{-N}(t)^T \quad \dots \quad \mathbf{z}_0(t)^T \quad \dots \quad \mathbf{z}_N(t)^T)^T \approx \Psi(t, \mathbf{y}(t)). \quad (13)$$

Correspondingly, due to $\mathbf{z}_k \approx e^{-ik\omega t}\mathbf{y}(t)$, the middle entry $\mathbf{z}_0(t)$ of the lifted state (13) directly approximates $\mathbf{y}(t)$. Going back from lifted coordinates \mathbf{z} to original coordinates $\mathbf{y} \approx \mathbf{z}_0 =: \mathbf{C}\mathbf{z}$ enables the approximation of arbitrary trajectories of (6) using the closed-form solution of the linear time-invariant lifted dynamics

$$\mathbf{y}(t) \approx \mathbf{z}_0(t) = \mathbf{C}e^{\mathbf{H}t}\mathbf{z}(0) = \mathbf{C}e^{\mathbf{H}t}\mathbf{W}\mathbf{y}(0) \quad (14)$$

given by the matrix exponential [12]. The matrix product $\mathbf{C}e^{\mathbf{H}t}\mathbf{W}$ in the expression (14) yields a matrix that (in approximation) maps any initial condition $\mathbf{y}(0)$ to the point on its trajectory after time t . Hence, it approximates the principal fundamental matrix $\Phi(t)$, cf. (7). In particular, an approximation of the monodromy matrix, i.e., the fundamental solution matrix evaluated at time T , can be identified from (14) as

$$\Phi_T \approx \mathbf{C}e^{\mathbf{H}T}\mathbf{W}. \quad (15)$$

The Floquet multipliers are then approximated by the eigenvalues of this matrix product.

The individual steps of this projection-based stability approach are visualized in Fig. 1. In this projection-based approach, the computationally intensive eigenvalue problem of the classical Hill methods is replaced by a matrix exponential. Various methods are available for efficient numerical calculation of matrix exponentials [31]. The classical ‘‘scaling and squaring’’ approach [32] exploits the fact that the Taylor series of $e^{\mathbf{H}t}$ is sufficiently accurate with only few summands if t is very small. Essentially, a small value t is chosen such that $T = 2^m t$ for some $m \in \mathbb{N}$, and then the desired result $e^{\mathbf{H}T}$ follows from the easier-to-compute intermediate result $e^{\mathbf{H}t}$ through m successive

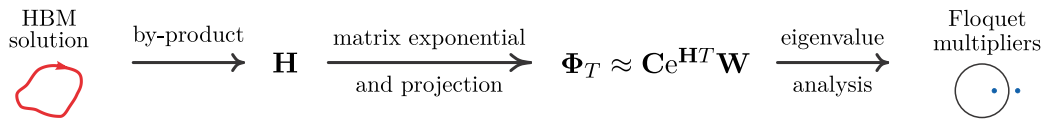


Fig. 1. Flowchart illustrating the Koopman-Hill projection stability method.

squaring operations. While still an operation of order $\mathcal{O}(N^3)$, the scaling and squaring approach benefits from sparse patterns in \mathbf{H} , unlike the solution of the eigenvalue problem. This is also how the built-in `expm` command of MATLAB implements the matrix exponential.

In (15), it suffices in principle to compute the action of the matrix exponential on the surrounding matrices, i.e., to obtain $\mathbf{C}e^{\mathbf{H}T}$ or $e^{\mathbf{H}T}\mathbf{W}$ immediately without determining the matrix exponential itself. In “scaling and squaring”-inspired Taylor series approaches [33,34], the repeated matrix–matrix multiplications of the first “scaling” step in the scaling and squaring approach are then replaced by matrix–vector multiplications for each column of \mathbf{W} (or row of \mathbf{C}), reducing memory requirements and computation time. However, as the resulting matrices are not square, the “squaring” step cannot be executed and the m squaring iterations are replaced by 2^m additional matrix–vector multiplications. This is beneficial if the number of columns of \mathbf{W} (or, analogously, rows of \mathbf{C}) is significantly smaller than the size of \mathbf{H} . In (15), the difference in size between \mathbf{H} and \mathbf{W} is determined only by the truncation order N . Usually, in application problems, N is chosen to be 20 or smaller, in which case the computational benefits of the squaring steps outweigh the benefits of the matrix–vector multiplication. Similar considerations also hold for other iterative matrix exponential solvers such as Krylov-based methods [35]. Therefore, the scaling and squaring approach given by `expm` is used in this work.

2.4. ANM continuation framework and quadratic equations

Commonly, the continuation problem for the algebraic residual (5) in dependence of a parameter $\lambda \in \mathbb{R}$ is solved by predictor–corrector methods [5,8,19,36]. In this paper, we consider the asymptotic numerical method (ANM), which solves continuation problems involving algebraic systems of the form (5) that have a certain quadratic structure without predictor–corrector steps. In the HBM context, the scalar control parameter λ can be the frequency or amplitude of the forcing [9], the energy of the system in free vibrations [4], or a simple parameter of the system in the case of self-excited oscillations [3], parameter variations [37] or continuation of points of special interest like bifurcation points [38] or antiresonances [39].

The following sections give a brief overview of the ANM continuation framework to motivate the benefits of the proposed differential quadratic recast of Section 3. Specific details about ANM can be found in [14–16], as well as in [40], where it is compared against predictor–corrector methods.

2.4.1. Continuation and ANM

Continuation seeks to find the solution \mathbf{X} of (5) as a function of a parameter λ . Because of fold bifurcation points, which create turning points in the branches of solutions plotted in the space (\mathbf{X}, λ) , the problem is locally re-parameterized as a function of a pseudo arc-length parameter a . Then, the ANM is based on a high-order Taylor series expansion of the solution branch such that $\tilde{\mathbf{X}} = (\mathbf{X}, \lambda)$ is expressed as a power series of a :

$$\tilde{\mathbf{X}}(a) = \tilde{\mathbf{X}}^{(0)} + a\tilde{\mathbf{X}}^{(1)} + a^2\tilde{\mathbf{X}}^{(2)} + \dots + a^P\tilde{\mathbf{X}}^{(P)}, \quad (16)$$

with $P \in \mathbb{N}$ the order of the series, that is chosen of the order $P = 20$ in practice. Then, the method consists of computing all coefficients $\tilde{\mathbf{X}}^{(p)}$ with $p = 1, 2, \dots, P$, for a given range of validity $a \in [0, a_{\max}]$ of the series (16), such that $\|\mathbf{R}(\mathbf{X}(a))\| < \epsilon$ for a user-specified tolerance $\epsilon \in \mathbb{R}$. A solution branch in the space (\mathbf{X}, λ) is expressed by a succession

of sections, each section given by $\tilde{\mathbf{X}}(a)$ for $a \in [0, a_{\max}]$ with $\tilde{\mathbf{X}}(a_{\max})$ serving as the starting point of the next section.

The computation of the coefficients of the power series (16) is particularly efficient if the nonlinear part of the algebraic system (5) contains quadratic polynomials only. In this case, each coefficient $\tilde{\mathbf{X}}^{(p)}$ is determined by a linear equation system. The system matrix is identical between all orders $p = 1, 2, \dots, P$, and the right-hand side for the p th coefficient only depends on the solution of the $p - 1$ previous systems, enabling a sequential computation of all desired coefficients. To bring the residue (4) into quadratic form, the dynamical system (1) must be recast into a quadratic form by introducing extra unknowns along with additional algebraic equations, resulting in differential algebraic equations (DAE). This operation, left in practice to the user, may appear restrictive at first sight, but is available for a large class of systems such as systems with polynomial nonlinearities (this case will be treated in the example of Section 2.4.2), and also systems with rational functions [41], transcendental functions [4,16] or constrained systems that are naturally written under DAE, like multibody systems [42] or large finite element geometrically exact beam models that include unitary quaternions [43].

An important feature of the ANM is that a_{\max} is automatically computed for a given tolerance ϵ in each section, thus enabling the computation of a solution branch with automatic step control. Moreover, if all power series coefficients $\tilde{\mathbf{X}}^{(p)}$ are stored for every section, the ANM has the benefit that not only the section end points $\tilde{\mathbf{X}}(0) = \tilde{\mathbf{X}}^{(0)}$ and $\tilde{\mathbf{X}}(a_{\max})$ are known to satisfactory exactness, but also all continuous points in between. Most other continuation methods do not possess this continuous resolution. As it is a HBM based method, the Hill matrix can be easily set up to compute the stability of the periodic solutions, as shown in Section 2.4.3. The ANM as explained here is implemented in an open-source software platform called Manlab, with graphical user interface capabilities. The public current version, Manlab 4.1.7 [44], has been taken as starting point for the implementation of the proposed stability technique and for all computations in the present paper.

2.4.2. Example 1a: Algebraic quadratic recast of a quintic nonlinear oscillator

To illustrate the algebraic quadratic recasting approach, we consider a nonlinear Duffing-type oscillator with quintic stiffness:

$$\ddot{x} + x + \epsilon\dot{x} + \alpha x^5 = F \cos \omega t. \quad (17)$$

The quintic nonlinearity αx^5 is initially not in quadratic form. However, by introducing new auxiliary states and corresponding constraints $z_1 = x_1^2, z_2 = x_1^3 = x_1 z_1$, the system can be written as a quadratic DAE

$$\dot{x}_1 = x_2 \quad (18a)$$

$$\dot{x}_2 = -x_1 - \epsilon x_2 - \alpha z_1 z_2 + F \cos \omega t \quad (18b)$$

$$0 = z_1 - x_1^2 \quad (18c)$$

$$0 = z_2 - x_1 z_1. \quad (18d)$$

Here, the auxiliary variables z_1, z_2 were chosen in a way that successively reduces the degree of the non-quadratic monomials involved, to arrive at (18) by an algebraic quadratic recast.

This procedure is not unique. For instance, an equivalent algebraic recast that still retains quadratic structure can be achieved by setting $\tilde{z}_2 = z_1^2$ and then using the equality $x_1^5 = x_1 x_1^4 = x_1 \tilde{z}_2$ in the differential equation (18b). The task of carrying out the algebraic quadratic recast

and selecting a pragmatic choice of auxiliary variables for an arbitrary problem at hand is usually left to the user [9].

In the recast (18), the so-called linear declaration rule [9,17] was employed: each auxiliary algebraic equation introduces one new auxiliary variable and may only depend on other auxiliary variables that were introduced in the equations above it. This ensures that the partial derivative of the auxiliary Eqs. (18c), (18d) with respect to \mathbf{z} has a lower triangular structure with ones on the diagonal, making it invertible [15, Section 4.3], [9].

2.4.3. Floquet–Hill stability computation

As introduced above, consider a dynamical system of the form (1) that was recast into the following quadratic DAE formalism:

$$\dot{\mathbf{x}} = \mathbf{f}_b(\mathbf{x}, \mathbf{z}) + \mathbf{g}_b(t) \quad (19a)$$

$$\mathbf{0} = \mathbf{f}_a(\mathbf{x}, \mathbf{z}) + \mathbf{g}_a(t), \quad (19b)$$

where $\mathbf{f}_b, \mathbf{f}_a$ are at most quadratic functions in (\mathbf{x}, \mathbf{z}) , by the introduction of new auxiliary variables $\mathbf{z} \in \mathbb{R}^a$ [14]. In particular, polynomial dynamics of arbitrary degree can be treated in a structured fashion that is illustrated exemplarily in the previous section.² To differentiate this classical procedure from the one introduced in Section 3, these recasting procedures that result in additional *algebraic* equations will be called *algebraic quadratic recast* in the following.

To find periodic solutions of (1), the HBM is applied to the $n = n_b + n_a$ differential algebraic Eqs. (19) to arrive at a set of $n(2N + 1)$ quadratic algebraic equations of the form (5), that can be written as

$$\omega \mathbf{D}\mathbf{X} = \mathbf{F}_b(\mathbf{X}, \mathbf{Z}) \quad (20a)$$

$$\mathbf{0} = \mathbf{F}_a(\mathbf{X}, \mathbf{Z}), \quad (20b)$$

where ω is the frequency of the Fourier series, \mathbf{D} is a constant matrix corresponding to the time-differentiation operation, $(\mathbf{F}_b, \mathbf{F}_a)$ are two quadratic functions and (\mathbf{X}, \mathbf{Z}) gather the Fourier coefficients of $(\mathbf{x}(t), \mathbf{z}(t))$. The Fourier coefficients of the quadratic nonlinearity of (19) can be computed explicitly [14, Appendix A], so $(\mathbf{D}, \mathbf{F}_b, \mathbf{F}_a)$ can be assembled directly and no alternating frequency–time scheme is necessary in the ANM–HBM approach.

The fact that (19) is a DAE incurs some additional steps in the stability computation as the classical Floquet theory only holds for ODEs. A possible approach for the stability computation is to go back from the DAE to the underlying ODE (1) and assemble the Hill matrix entry by entry [10]. This is possible as, by the implicit function theorem, there is an implicit relationship $\mathbf{z}(t) = \mathbf{z}(\mathbf{x}(t), t)$ given by \mathbf{f}_a if $\partial \mathbf{f}_a / \partial \mathbf{z}$ is invertible, relating \mathbf{f}_b and the original ODE (1) by substitution. The invertibility can for instance be ensured by the linear declaration rule, cf. Section 2.4.2. However, it also works in other more complex cases for which $\mathbf{f}_a(\mathbf{x}, \mathbf{z}, t)$ is a general quadratic function, in the case of regularized friction laws for instance [40,41].

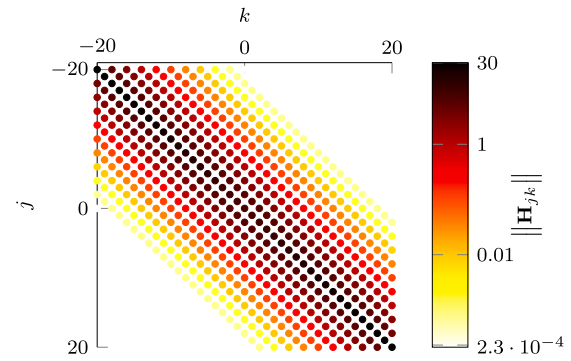
This substitution can also be carried out directly in the frequency domain [9], yielding the Hill matrix as a function of the Jacobians of the HBM algebraic system (20) computed at the periodic solution $\mathbf{x}^p(t)$. Equation (20b) implicitly defines $\mathbf{Z} = \mathbf{Z}(\mathbf{X})$ and its partial derivative

$$\frac{\partial \mathbf{Z}(\mathbf{X})}{\partial \mathbf{X}} = - \left(\frac{\partial \mathbf{F}_a}{\partial \mathbf{Z}} \right)^{-1} \frac{\partial \mathbf{F}_a}{\partial \mathbf{X}}, \quad (21)$$

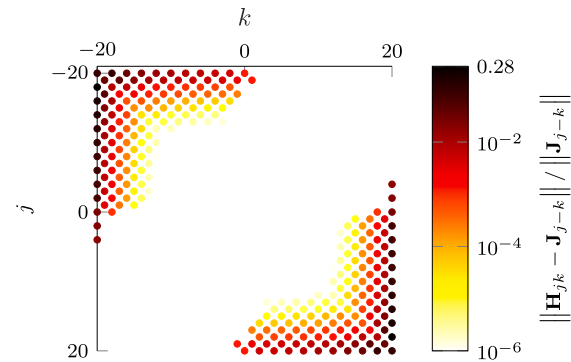
enabling the computation of the Hill matrix:

$$\begin{aligned} \mathbf{H} &\approx \frac{\partial}{\partial \mathbf{X}} \mathbf{F}_b(\mathbf{X}, \mathbf{Z}(\mathbf{X})) - \omega \mathbf{D} \\ &= \frac{\partial \mathbf{F}_b}{\partial \mathbf{X}} - \frac{\partial \mathbf{F}_b}{\partial \mathbf{Z}} \left(\frac{\partial \mathbf{F}_a}{\partial \mathbf{Z}} \right)^{-1} \frac{\partial \mathbf{F}_a}{\partial \mathbf{X}} - \omega \mathbf{D}. \end{aligned} \quad (22)$$

² For general transcendental nonlinearities, it is sometimes necessary to express (19) in a differentiated format, explicitly treating the initial conditions of the constraints [17]. This *algebraic quadratic recast in differentiated form* is not considered in this work as it is not necessary for polynomial nonlinearities.



(a) Norm of the Hill matrix block entries revealing (approximate) block-Toeplitz structure.



(b) Relative error of the Hill matrix block entries due to truncation effects in the condensation operation.

Fig. 2. Hill matrix of order $N = 20$ and truncation effects for the algebraically recast Duffing oscillator (18) with $\omega = 1.35$, $\alpha = 1$, $F = 3$, $\epsilon = 0.25$.

If the linear declaration rule is observed, the Jacobian $\partial \mathbf{F}_a / \partial \mathbf{Z}$ is lower triangular and invertible as well. Consequently, after the periodic solution $(\mathbf{X}^p, \mathbf{Z}^p)$ is found using HBM, the Hill matrix can be computed using the above condensation operation in order to compute the stability, as explained in [9,10] and Section 2.2. As an example, Fig. 2(a) shows the norm of each block entry of \mathbf{H} for a Hill matrix of the quintic Duffing example of Section 2.4.2, computed using the algebraic quadratic recast (18) and the condensation operation (22) with the parameters $\omega = 1.35$, $\alpha = 1$, $F = 3$, and $\epsilon = 0.25$. The banded block Toeplitz structure that is expected from the Hill matrix appears to be visible: Entries that lie on the same diagonal have approximately the same norm, which decays towards the corners.³

However, a closer inspection reveals that the condensation operation (22) in the frequency domain causes truncation effects towards the edges of the Hill matrix that deteriorate the block Toeplitz structure. For the Hill matrix, all blocks $\mathbf{H}_{j+l, k+l}$ that lie on the same diagonal are expected to have the identical value \mathbf{J}_{j-k} , cf. Section 2.2. For every block diagonal, we take the most centered block as reference \mathbf{J}_{j-k} . Fig. 2(b) shows the relative difference between these reference blocks and other blocks on the same diagonal, expected to have the identical value. Towards the outer edges of the matrix, this error is significant, up to almost 30%. A possible explanation is due to truncation effects in the algebraic auxiliary variables. Any function $\mathbf{x}(t)$ parameterized

³ Along the main diagonal, there are additional terms of the form $ik\omega$, which are expected to vary. The Hill matrix is thus not block Toeplitz in the strict sense, however in the present section we are mainly interested in effects that concern the off-diagonal components of \mathbf{H} and use the wording “block Toeplitz” accordingly.

by its Fourier coefficients \mathbf{X} is implicitly assumed to have bandwidth N , i.e., frequency components outside the truncation order N are assumed to be zero. However, this is not necessarily also the case for the signal $\mathbf{z}(\mathbf{x}(t), t)$ implicitly defined by the relationship between base and auxiliary variables. The frequency components of $\mathbf{z}(\mathbf{x}(t), t)$ outside the admissible range are not reflected in $\mathbf{Z}(\mathbf{X})$, potentially leading to the truncation effects in (22).

In the symmetry-based stability approach of [9,10] that is classically employed in the ANM, the Floquet exponents are determined as those eigenvalues of \mathbf{H} with the most symmetrical eigenvectors, which are usually characterized by large values in the center and small values towards the edges [10]. For this reason, they are not significantly affected by the deterioration of the Toeplitz structure, which mainly impacts the outermost columns of the computed Hill matrix, cf. Fig. 2(b). In contrast, the matrix exponential of the Koopman–Hill stability method involves all rows of the Hill matrix equally, making it more sensitive to effects that deteriorate the expected block Toeplitz structure.

3. Differential quadratic recast for polynomial dynamics

As detailed in the previous sections, the Hill matrix for a system in DAE form produced by the algebraic quadratic recast suffers from truncation effects, impacting the accuracy of the Koopman–Hill projection method. To avoid the condensation step (22), a quadratic recast procedure which results in an ordinary differential equation without any additional algebraic equations is sought.

The so-called *exact quadratization* (EQ) problem has been treated in the literature for polynomials [45] and also for larger system classes [46,47]. In contrast to the algebraic recast, the auxiliary equations are defined in differentiated form, yielding a set of ODEs, together with constraints on their initial conditions. This is sufficient for numerical forward integration in time, when the extended state is constrained by the initial condition to a physically meaningful manifold. In the ANM–HBM continuation procedure, however, initial conditions are only implicitly determined by the unknown Fourier coefficients with no guarantee on satisfying any additional constraints. It is therefore necessary to enforce physical meaning for all solutions that can be admitted by the ANM–HBM procedure. This could be dealt with similarly as non-polynomial nonlinearities are treated in [4,17]: for each auxiliary variable, one of its HBM equations is replaced by its corresponding initial condition. Similarly as with the algebraic recast above, additional steps would then be necessary to reconstruct the correct Hill matrix from the Jacobian of these modified HBM equations, adding computational effort and limiting interpretability.

Alternatively, the auxiliary states could be designed in such a fashion that solutions retain desirable properties even outside the physically meaningful manifold. In [48], a *dissipativity-preserving quadratization* is proposed which retains the stability properties of equilibria of the original dynamics even outside the physically meaningful manifold. With a similar aim but for arbitrary stationary solutions, we propose a *differential quadratic recast* procedure for polynomial dynamics based on a Baumgarte-like stabilization that arrives at a larger ODE (like the EQ would), adding only differential auxiliary equations instead of algebraic ones. The proposed differential recast guarantees that there do not exist any spurious stationary solutions for arbitrary initial conditions and ensures that all solutions converge to the physically meaningful manifold. This leaves ANM–HBM applicability unchanged while also directly making the Hill matrix and Floquet theory applicable without any prior inversions or substitutions. In many practical cases (for example mechanical systems with linear kinematics and nonlinearities of degree less than five), the resulting number of unknowns and, thus, the computational effort of the HBM with ANM will be identical between algebraic and differential recast.

3.1. Example 1b: Differential quadratic recast of a quintic nonlinear oscillator

Before treating general polynomial nonlinearities, we revisit the nonlinear Duffing-type oscillator with polynomial stiffness of degree 5 (17) of Section 2.4.2. The differential quadratic recast strives to arrive at a system of purely differential equations without algebraic constraints which resembles the DAE (18) as much as possible. To soften the algebraic conditions (18c), (18d), an error $\mathbf{e} := (e_1, e_2)^T$ with

$$e_1 = z_1 - x_1^2 \quad (23a)$$

$$e_2 = z_2 - x_1^3 \quad (23b)$$

as a function of (\mathbf{x}, \mathbf{z}) is introduced. Algebraically requiring $\mathbf{e} = \mathbf{0}$, we recover identically the algebraic recast (18). For the differential quadratic recast, we instead set up globally asymptotically stable error dynamics

$$\dot{\mathbf{e}} = -k\mathbf{e}, \quad (24)$$

inspired by the Baumgarte stabilization approach for the numerical integration of DAEs [49]. The linear ODE (24) is decoupled from the system dynamics and its unique stationary solution is $\mathbf{e} \equiv \mathbf{0}$. Expressing \mathbf{e} and $\dot{\mathbf{e}}$ again in (\mathbf{x}, \mathbf{z}) using (23), we arrive at the equivalent dynamical system

$$\dot{x}_1 = x_2 \quad (25a)$$

$$\dot{x}_2 = -x_1 - \varepsilon x_2 - \alpha z_1 z_2 + F \cos \omega t \quad (25b)$$

$$\dot{z}_1 = \dot{e}_1 + 2x_1 \dot{x}_1 = 2x_1 x_2 - k(z_1 - x_1^2) \quad (25c)$$

$$\dot{z}_2 = \dot{e}_2 + 3x_1^2 \dot{x}_1 = 3x_1^2 x_2 - k(z_2 - x_1^3). \quad (25d)$$

System (25) is an ODE with states $(\mathbf{x}^T, \mathbf{z}^T)^T$, of which any solution converges asymptotically to the manifold $z_1 = x_1^2$, $z_2 = x_1^3$ due to (24), independent of its initial condition. Stationary solutions of (25) are therefore equivalent to stationary solutions of (17). Still, (25) is not a dynamical system in quadratic form as cubic nonlinearities remain in the auxiliary equations. However, on the periodic solution of (25), $e_1 \equiv 0$ and thus $z_1 \equiv x_1^2$ holds. Intuitively, this allows to also substitute x_1^2 by z_1 in (25d), retaining the identical periodic solution and yielding the modified z_2 dynamics

$$\dot{z}_2 = 3z_1 x_2 - k(z_2 - x_1 z_1). \quad (26)$$

The differential quadratic recast (25a)–(25c) with (26) indeed only admits quadratic nonlinearities. Observe that the linear declaration rule is still fulfilled: The linearization matrix $\frac{\partial \dot{\mathbf{z}}}{\partial \mathbf{z}}$ is a lower triangular matrix with $-k$ on the diagonal.

The choice of $k > 0$ is arbitrary and only weak practical restrictions apply. For $k = \infty$, the differential quadratic recast becomes equivalent to the algebraic quadratic recast, but an excessively large choice of k results in a numerically stiff ODE. In contrast, a very small magnitude of k results in a weak attraction to the manifold. Fig. 3(a) depicts frequency response curves (FRC) for the quintic Duffing oscillator determined using the MANLAB toolbox with the differential recast (25a)–(25c) with (26) or the algebraic recast (18), with harmonic truncation order $N = 20$ and varying choices of k in the differential recast. For values of $k \geq 0.002$, the approximation of the FRC is virtually identical between differential and algebraic recast. For a very small value $k = 0.001$, however, the FRC curve obtained by the differential recast is inaccurate. This inaccuracy is reflected in the discrepancy between the auxiliary variable z_2 and the nonlinear function x_1^3 that it approximates, visible in Fig. 3(b), making this discrepancy a suitable error measure that could be monitored during the ANM computations. Fig. 3(c) shows the Floquet multipliers at $\omega = 1.35$ obtained from the different recasts. The Floquet multipliers of the original problem are represented well by all recasts except for $k = 0.001$. Additionally, all differential recasts admit Floquet multipliers at e^{-kT} , which is close to zero for $k = 5$ and close to one for $k = 0.001$ and $k = 0.002$. In practice, k should be

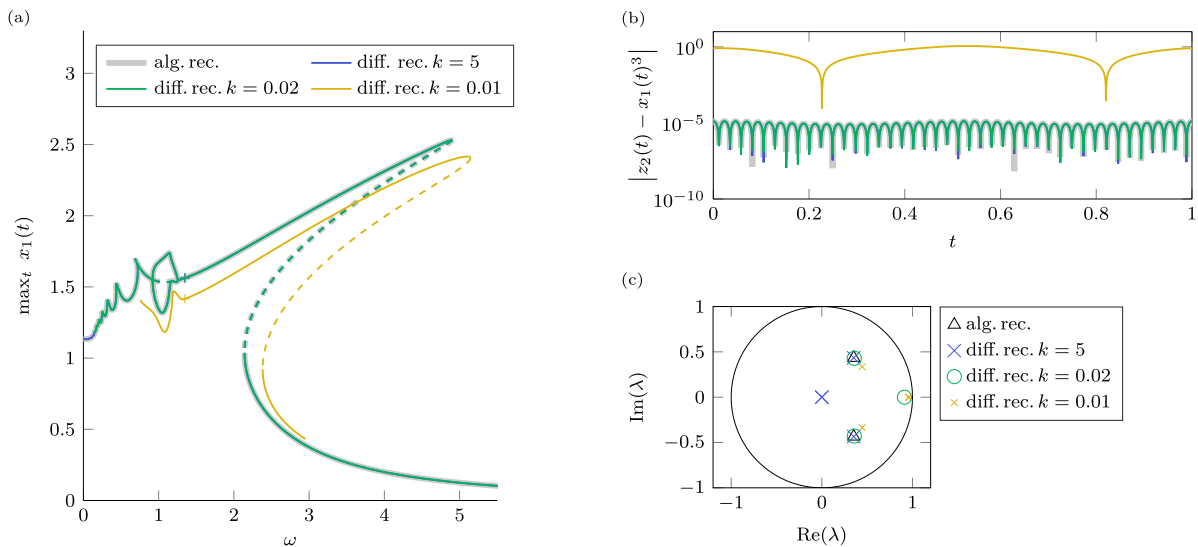


Fig. 3. Quintic Duffing oscillator computed in MANLAB using algebraic or differential recast with $\alpha = 1$, $\epsilon = 0.05$, $N = 20$ and various values for k . (a) Frequency response curves. Unstable branches are depicted by dashed lines, and stable branches by solid lines. (b) Error between auxiliary variable z_2 and approximated value x_1^3 for the periodic solution at $\omega = 1.35$. (c) Floquet multipliers for the periodic solution at $\omega = 1.35$.

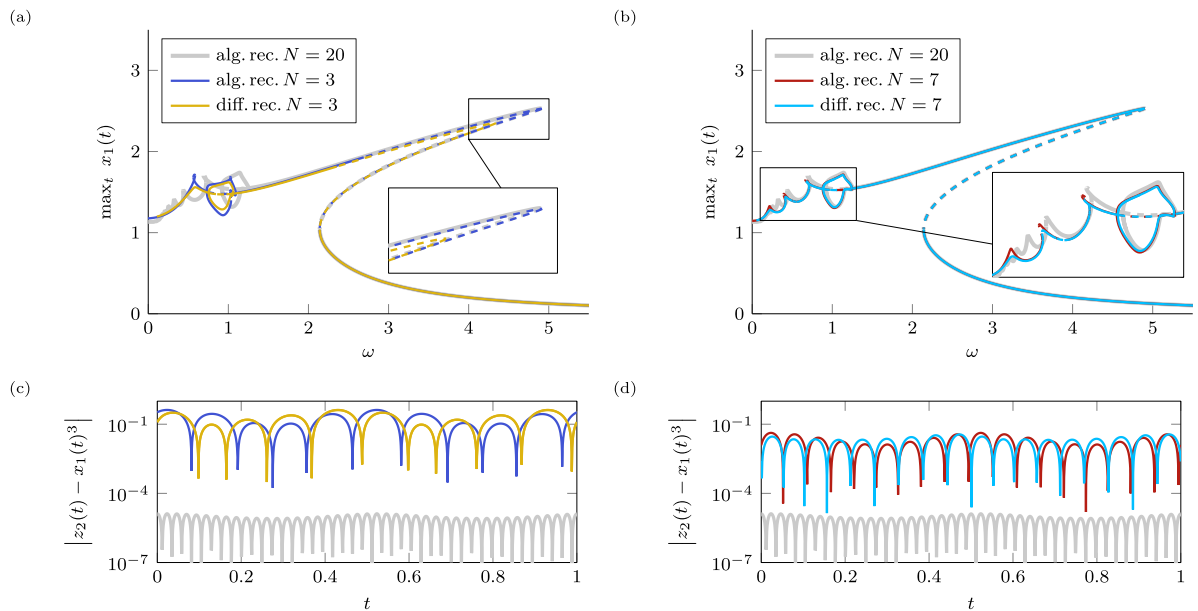


Fig. 4. Quintic Duffing oscillator computed in MANLAB using algebraic and differential recast with $\alpha = 1$, $\epsilon = 0.05$, $k = 5$ and various values for N . (a) Frequency response curve for $N = 3$. Unstable branches are depicted by dashed lines, and stable branches by solid lines. (c) Error between auxiliary variable z_2 and approximated value x_1^3 for the periodic solution at $\omega = 1.35$ with $N = 3$. (b) Frequency response curve for $N = 7$. Unstable branches are depicted by dashed lines, and stable branches by solid lines. (d) Error between auxiliary variable z_2 and approximated value x_1^3 for the periodic solution at $\omega = 1.35$ with $N = 7$.

chosen depending on the period time T such that the resulting Floquet multiplier is not close to 1, but k should also not be chosen exorbitantly large to avoid additional stiffness being introduced into the system. Below, we fix the value $k = 5$, which is appropriate in this sense.

In Fig. 4, the properties of the differential and algebraic recast are compared for various truncation orders N . For a very small truncation order ($N = 3$) shown in Fig. 4(a), both FRCs determined using the differential and the algebraic quadratic recast, respectively, show the hardening behavior of the Duffing oscillator but are inaccurate. While the algebraic recast finds the turning point of the main branch at approximately the right frequency with slightly increased amplitude, the turning point found by the differential recast is earlier at $\omega \approx 4.5$. With the symmetry-based sorting approach [9] for stability determination, both recasting approaches find a spurious Neimark–Sacker bifurcation

at $\omega \approx 2.35$ and $\omega \approx 2.7$, respectively, which falsely classifies a large part of the main branch as unstable. This is not due to the recast, but rather due to the insufficient approximation order in the HBM. Both approaches do find symmetry-breaking bifurcations around $\omega = 1$ and allow to track asymmetric branches, however both the differential and the algebraic recast with $N = 3$ show significant discrepancies with the reference solution $N = 20$. The error between the auxiliary variable z_2 and its expected value x_1^3 , shown in Fig. 4(c) is of the order 10^{-1} for both approaches, reflecting the insufficient accuracy.

In contrast, with truncation order $N = 7$, both approaches trace the main branch perfectly as shown in Fig. 4(b), with correct stability assertions. The asymmetric branches at $\omega \approx 1$ are not tracked perfectly at this truncation order by any of the two approaches, but the branches determined by the two approaches overlap almost completely.

This shows that both recasting approaches are not mathematically equivalent, but have very similar convergence behavior.

3.2. General polynomial recast

In the above example, the introduction of auxiliary variables with globally asymptotically stable error dynamics allowed to reduce the degree of the polynomial nonlinearity, yielding a quadratic ODE. This idea can be generalized to arbitrary polynomial nonlinearities.

Below, we use multi-indices $\beta \in \mathbb{N}^{n_b}$ with a norm $|\beta| := \sum_{i=1}^{n_b} \beta_i$, allowing to concisely write scalar monomials $\mathbf{x}^\beta := \prod_{i=1}^{n_b} x_i^{\beta_i}$ of degree $|\beta|$. The monomial \mathbf{x}^β is scalar, while both its operands \mathbf{x} , β are vector-valued quantities. The i th unit vector \mathbf{e}_i can be regarded as a multi-index with norm 1 and $\mathbf{x}^{\mathbf{e}_i} = x_i$.

Consider an arbitrary dynamical system in polynomial form

$$\dot{\mathbf{x}} = \mathbf{f}(\mathbf{x}, t) = \mathbf{A}\mathbf{x} + \sum_{2 \leq |\beta| \leq m} \mathbf{h}_\beta \mathbf{x}^\beta + \mathbf{g}(t) \quad (27)$$

with state $\mathbf{x} \in \mathbb{R}^{n_b}$, possibly time-dependent (or constant) T -periodic components $\mathbf{g}(t)$, a linearization matrix \mathbf{A} and coefficients \mathbf{h}_β for polynomial nonlinearities up to degree m . In the spirit of (23), we introduce for every considered monomial \mathbf{x}^β of degree 2 or more the auxiliary state z_β and the corresponding error e_β by

$$e_\beta := z_\beta - \mathbf{x}^\beta \quad 2 \leq |\beta| \leq m. \quad (28)$$

The vectors \mathbf{e} , \mathbf{z} collect these auxiliary states and errors and are ordered via $\mathbf{e}^T = (e_{\beta(1)}, \dots, e_{\beta(n_a)})^T$ in ascending order of $|\beta|$. The vector of error coordinates \mathbf{e} must not be confused with a unit vector \mathbf{e}_i . Constructed in this fashion, \mathbf{e} and \mathbf{z} have a potentially very large length $n_a := \binom{m+n_b}{n_b} - (n_b + 1)$, however, Section 3.3 details a procedure to reduce the number of auxiliary equations for many practical cases. For each auxiliary state, we set up identical error dynamics $\dot{e}_\beta = -k e_\beta$, $k > 0$, which, substituted into (28), yields the dynamics

$$\begin{aligned} \dot{z}_\beta &= \frac{d}{dt} (e_\beta + \mathbf{x}^\beta) \\ &= -k(z_\beta - \mathbf{x}^\beta) + \sum_{j=1}^{n_b} \beta_j \mathbf{x}^{\beta - \mathbf{e}_j} f_j(\mathbf{x}, t), \quad 2 \leq |\beta| \leq m. \end{aligned} \quad (29)$$

Solutions of the coupled dynamics (27), (29) converge asymptotically towards $e_\beta = 0$ or, equivalently, $z_\beta = \mathbf{x}^\beta$ for all considered β . The manifold $\mathbf{e} \equiv \mathbf{0}$, or, equivalently, $z_\beta = \mathbf{x}^\beta$ for all β , is invariant and globally asymptotically stable.

To arrive at a quadratic differential equation, higher-degree monomials of \mathbf{x} in (27) and (29) are replaced by their corresponding auxiliary state z_β . The auxiliary dynamics (29) contains products of the form $\mathbf{x}^{\beta - \mathbf{e}_j} f_j(\mathbf{x}, t)$ which can only be put in quadratic form if both factors are linear. Linearity of the first factor is immediately given through substitution of $\mathbf{x}^{\beta - \mathbf{e}_j}$ with $z_{\beta - \mathbf{e}_j}$. To ensure linearity of the second factor, i.e., the original dynamics, each monomial term of the form \mathbf{x}^β in (27) is replaced by its corresponding auxiliary state z_β .

The only other potentially higher-degree monomial term that occurs in (29) is \mathbf{x}^β . For $|\beta| = 2$, this is a quadratic term and no substitutions are needed. For $|\beta| > 2$, the monomial can be split into the product $\mathbf{x}^\beta = x_l \mathbf{x}^{\beta - \mathbf{e}_l}$ for $l \in \{1, \dots, n_b\}$ such that $\beta - \mathbf{e}_l$ is a multi-index of norm $|\beta| - 1$. The chosen index l does not influence approximation behavior. Then, $\mathbf{x}^{\beta - \mathbf{e}_l}$ can be substituted by the corresponding auxiliary variable $z_{\beta - \mathbf{e}_l}$. In summary, the substitution of all higher-degree monomials by their corresponding auxiliary variables yields

$$\dot{\mathbf{x}} = \tilde{\mathbf{f}}(\mathbf{x}, \mathbf{z}, t) := \mathbf{A}\mathbf{x} + \sum_{2 \leq |\beta| \leq m} \mathbf{h}_\beta z_\beta + \mathbf{g}(t) \quad (30a)$$

$$\dot{z}_\beta = -k(z_\beta - \mathbf{x}^\beta) + \sum_{j=1}^{n_b} \beta_j \mathbf{x}^{\beta - \mathbf{e}_j} \tilde{f}_j(\mathbf{x}, \mathbf{z}, t), \quad |\beta| = 2 \quad (30b)$$

$$\dot{z}_\beta = -k(z_\beta - x_l z_{\beta - \mathbf{e}_l}) + \sum_{j=1}^{n_b} \beta_j z_{\beta - \mathbf{e}_j} \tilde{f}_j(\mathbf{x}, \mathbf{z}, t), \quad 3 \leq |\beta| \leq m. \quad (30c)$$

All summands of (30) are at most quadratic in (\mathbf{x}, \mathbf{z}) , making this a quadratic ordinary differential equation that can be treated using ANM. The transient dynamics of the original system (27) and the DAE (19) resulting from an algebraic recast are equivalent [14]. Due to the substitutions, this is not true for the transient dynamics of the differential recast (30), which will generally differ while the error dynamically converges to zero. However, as the manifold characterized by $\mathbf{z}_\beta = \mathbf{x}^\beta$ for all β is invariant, and the error is asymptotically autonomous, stationary solutions of (30) always coincide with those of (27). Intuitively, this is due to the lower triangular structure of (30c), which ensures that the error dynamics of each monomial degree decouples from higher degrees and has zero as its only stationary solution. All auxiliary Eqs. (30b), (30c) hence produce additional Floquet exponents at $-k$. A full proof of these statements is detailed in Appendix A.

Using the error \mathbf{e} to stabilize the dynamics off the physically meaningful manifold is an approach that was also recently proposed in [48]. While the construction of [48] does not require the original dynamics to be linear in the auxiliary variables, leading to fewer auxiliary equations than the approach presented here, it requires an iterative procedure that involves checking the stability of the complete extended system at each iteration to come up with a stability-preserving quadratization. This makes the approach of [48] unsuitable for the application inside the ANM-HBM framework, where this stability computation is already the bottleneck and further stability computation steps would lead to an excessive amount of computational effort.

3.3. Reduction of auxiliary variables

The differential recast procedure of Section 3.2 yields a system of quadratic ordinary differential equations for arbitrary polynomial dynamics. However, this recast in its general form (30) relies on introducing auxiliary variables for every monomial between degree 2 and the maximum polynomial degree m of the original dynamics. The maximum number of auxiliary variables in the most general form is $n_a = \binom{m+n_b}{n_b} - (n_b + 1)$, which increases with $m!$ and is therefore prohibitive to the applicability of the approach for polynomial nonlinearities of large degree.

Usually in practice, not all states are nonlinearly coupled to each other, so many of the factors \mathbf{h}_β vanish. To reduce the number of auxiliary states, it is only necessary to construct z_β for such β where \mathbf{h}_β does not vanish. Additionally, to guarantee that (30c) is well-defined, auxiliary states $z_{\beta - \mathbf{e}_j}$ must be kept as long as $\beta - \mathbf{e}_j$ is a multi-index of norm 2 or higher to be able to evaluate the sum expression in (30c).

Further reduction is possible for mechanical systems of the form

$$\dot{\mathbf{q}} = \mathbf{u} \quad (31a)$$

$$\mathbf{M}\dot{\mathbf{u}} + \mathbf{D}\mathbf{u} + \mathbf{K}\mathbf{q} + \sum_{|\gamma|=2} \mathbf{n}_\gamma \mathbf{u}^\gamma + \sum_{2 \leq |\beta| \leq m} \mathbf{h}_\beta \mathbf{q}^\beta = \mathbf{g}(t), \quad (31b)$$

where $\mathbf{q} \in \mathbb{R}^{\frac{n_b}{2}}$ is a set of minimal position-level coordinates and \mathbf{u} the corresponding minimal velocities and $\mathbf{M}, \mathbf{D}, \mathbf{K}$ are constant matrices. Nonlinearities on the velocity level appear at most quadratically, and nonlinearities on position level can be polynomial of arbitrary degree. This system class allows to study many problems of interest in structural dynamics, such as vibrations of geometrically nonlinear elastic structures, for which the stiffness nonlinearities are polynomials at most cubic, or reduced dynamics of those structures using invariant manifolds, for which the nonlinearities are polynomial at an arbitrary order [42,50,51]. The quintic Duffing oscillator of Section 3.1 is also of this system class.

The nonlinearities in \mathbf{u} are already quadratic, so auxiliary variables are only needed for monomials on position level \mathbf{q} . In (30c), products of auxiliary variables $z_{\beta - \mathbf{e}_j}$ with the corresponding state dynamics \tilde{f}_j occur, necessitating the linearity of (30a) to ensure that the resulting product is at most quadratic. As the kinematic equation (31a) is linear already before the recast, (30c) will be at most quadratic for any

z_β approximating position-dependent terms only, irrespective of the nonlinearities in the kinetic Eqs. (31b). This alleviates the necessity to bring (31b) into linear form; a quadratic form is sufficient.

The differential quadratic recast then admits the form

$$\dot{\mathbf{q}} = \mathbf{u} \quad (32a)$$

$$\mathbf{M}\dot{\mathbf{u}} = -\mathbf{D}\mathbf{u} - \mathbf{K}\mathbf{q} - \sum_{|\gamma|=2} \mathbf{n}_\gamma \mathbf{u}^\gamma - \sum_{\substack{2 \leq |\beta| \leq \lfloor \frac{m}{2} \rfloor \\ 2 \leq |\xi| \leq \lfloor \frac{m}{2} \rfloor}} \mathbf{h}_{(\beta+\xi)} z_\beta z_\xi + \mathbf{g}(t) \quad (32b)$$

$$\dot{z}_\beta = -k(z_\beta - \mathbf{q}^\beta) + \sum_{j=1}^{\frac{n_b}{2}} \beta_j u_j \mathbf{q}^{\beta-e_j}, \quad |\beta| = 2 \quad (32c)$$

$$\dot{z}_\beta = -k(z_\beta - q_l z_{\beta-e_l}) + \sum_{j=1}^{\frac{n_b}{2}} \beta_j u_j z_{\beta-e_j}, \quad 3 \leq |\beta| \leq \lfloor \frac{m}{2} \rfloor. \quad (32d)$$

As above, l is chosen for every considered β such that $\beta - e_l$ is a multi-index of degree 2 or more. In particular, the auxiliary variables only encode monomials up to degree $\lfloor \frac{m}{2} \rfloor$. Due to the nonlinear increase of monomials per degree, this greatly reduces the number of auxiliary variables. In many low-degree cases, such as cubic and quartic monomials or monomials of only one variable up to degree 7, this differential recast admits the same number of auxiliary variables as needed for the algebraic recast. This is in particular also the case for the slender geometrically nonlinear beam examples of Section 5.

4. The Hill matrix for real-valued Fourier series

Both real-valued and complex-valued Fourier series may be employed in the HBM and yield complex and real representations of the Hill matrix, respectively. The classical Hill determinant interpretation of Section 2.2 as an eigenvalue problem for the Floquet form (10) with complex-valued Fourier series is well-known [6,10,11,18,22]. Also, the Koopman–Hill projection method (cf. Section 2.3) has until now only been developed and proven for this Hill matrix in complex form. However, for practical reasons, the harmonic balance method is often implemented in its real-valued form, as it is for example also in the MANLAB framework. Therefore, one either needs to re-derive all frequency-based stability methods for the real-valued case (for instance, an expression for a real-valued Hill matrix was given in [11]), or use transformations between the real- and complex-valued representations.

The first option, re-deriving the theory, has (partially) been done [9, 11] for the Hill matrix, but the necessary algebraic calculation steps as well as the resulting matrix are significantly more involved and error-prone than in the classical complex-valued case due to cumbersome trigonometric identities. Additionally, the more complicated matrix structure in the real-valued case limits the interpretability of the results. An explicit variant of the Koopman–Hill projection algorithm with a real-valued lift has not yet been addressed in the literature.

In this work, we will take the other path and re-derive a generalized view of the Hill matrix as the derivative of the HBM equations, independent of the chosen Fourier basis. This view is well-known in the literature [9,40], but the specific generalized proof below is novel to the knowledge of the authors. This generalized view immediately provides linear transformations between equivalent Hill matrices for different Fourier bases, allowing to switch easily, quickly, and robustly between real and complex basis formulations. We will then use this unified view to generalize the Koopman–Hill projection approach to arbitrary real-valued Hill matrix formulations in Section 4.3, making it immediately available in real-valued HBM settings.

4.1. The Hill matrix as Jacobian of the HBM

In this section we will introduce a generalization of the classical procedure [10,11,18] to arrive at Hill's eigenvalue problem, assuming as little structure of the Fourier basis functions as possible. As

introduced in Section 2.1, we consider a matrix $\mathbf{U}(t) = \mathbf{u}(t) \otimes \mathbf{I}_{n \times n} \in \mathbb{C}^{n(2N+1) \times n}$ where \mathbf{u} is a column vector of length $2N+1$ that collects a set of orthonormal Fourier basis functions up to order N , e.g. functions of the form $e^{ik\omega t}$ or $\cos k\omega t$. Two exemplary choices for \mathbf{U} are given in Appendix B. The Kronecker product ensures that \mathbf{U} provides the corresponding Fourier basis for n -dimensional space such that for a periodic signal $\mathbf{x}(t) \in \mathbb{R}^n$ of finite bandwidth N with Fourier coefficients $\mathbf{X} \in \mathbb{C}^{n(2N+1)}$, the Fourier synthesis equation

$$\mathbf{x}(t) = \sum_k u_k(t) \mathbf{X}_k = \mathbf{U}(t)^T \mathbf{X} \quad (33)$$

holds. The Fourier analysis equation, i.e., the equation to determine the Fourier coefficients given a function $\mathbf{x}(t)$, is classically expressed in terms of an inner product involving the complex conjugate. However, for this work it is imperative to express the Fourier analysis explicitly as the integral

$$\mathbf{X} = \mathcal{F}_N(\mathbf{x}) := \frac{1}{T} \int_0^T \mathbf{U}^*(t) \mathbf{x}(t) dt \quad (34)$$

where $\mathbf{U}^* \in \mathbb{C}^{n(2N+1) \times n}$ with $\frac{1}{T} \int_0^T \mathbf{U}^*(t) \mathbf{U}(t)^T dt = \mathbf{I}$ is chosen such that it reflects this conjugation process [52]. The Fourier analysis equation (34) is not restricted to vector-valued functions $\mathbf{x}(t) \in \mathbb{C}^n$. It may also be applied to matrix-valued functions in $\mathbb{C}^{n \times m}$ for arbitrary m . Appendix B lists explicit formulations of \mathbf{U} and \mathbf{U}^* in common complex and real cases. By definition, the matrix \mathbf{U} is T -periodic with $T = \frac{2\pi}{\omega}$ and has a derivative

$$\frac{d\mathbf{U}(t)^T}{dt} = \mathbf{U}(t)^T \omega \mathbf{D}, \quad (35)$$

where \mathbf{D} is a sparse, constant, and not necessarily symmetric matrix that is known a priori and only depends on the choice of \mathbf{U} . Examples for \mathbf{D} are also given in Appendix B.

As introduced in Section 2.1, the HBM equations are defined by the Fourier coefficients up to order N of the dynamic residual of (1). Expressing $\mathbf{x}(t) = \mathbf{U}(t)^T \mathbf{X}$ and $\dot{\mathbf{x}}(t) = \frac{d}{dt} (\mathbf{U}(t)^T \mathbf{X}) = \mathbf{U}(t)^T \omega \mathbf{D} \mathbf{X}$, we can write this residual as

$$\begin{aligned} \mathbf{R}(\mathbf{X}) &= \mathcal{F}_N(\mathbf{f}(\mathbf{x}, t) - \dot{\mathbf{x}}) \\ &= \frac{1}{T} \int_0^T \mathbf{U}^* (\mathbf{f}(\mathbf{U}^T \mathbf{X}, t) - \mathbf{U}^T \omega \mathbf{D} \mathbf{X}) dt \end{aligned} \quad (36)$$

where dependencies on t were omitted for the sake of brevity. Consequently, the Jacobian of the HBM equations is given by the partial derivative of (36)

$$\begin{aligned} \mathbf{H} &:= \frac{\partial \mathbf{R}}{\partial \mathbf{X}} \\ &= -\frac{1}{T} \int_0^T \mathbf{U}^* \mathbf{U}^T dt \omega \mathbf{D} + \frac{1}{T} \int_0^T \mathbf{U}^* \left. \frac{\partial \mathbf{f}}{\partial \mathbf{x}} \right|_{\mathbf{U}^T \mathbf{X}} \mathbf{U}^T dt \\ &= -\omega \mathbf{D} + \mathcal{F}_N(\mathbf{J}(t) \mathbf{U}^T) \end{aligned} \quad (37)$$

with $\mathbf{J}(t) = \left. \frac{\partial \mathbf{f}(\mathbf{x}, t)}{\partial \mathbf{x}} \right|_{\mathbf{U}^T \mathbf{X}}$, cf. (6). The partial derivative (37) will be called \mathbf{H} preemptively as we will show below that it is indeed the expected Hill matrix.

We will now proceed analogously to [10] in this generalized form to show that the matrix \mathbf{H} is indeed the finite truncation of the infinite Hill eigenvalue problem. Consider a Floquet form solution (10) with Floquet exponent α . Its periodic component has a truncated Fourier series representation $\mathbf{p}(t) = \mathbf{U}(t)^T \mathbf{P}$ with $\mathbf{P} \in \mathbb{C}^{n(2N+1)}$ being the vector of its Fourier coefficients. We can express the Floquet form solution and its derivative by

$$\mathbf{y}(t) = \mathbf{U}(t)^T \mathbf{P} e^{\alpha t} \quad (38)$$

$$\dot{\mathbf{y}}(t) = \mathbf{U}(t)^T (\omega \mathbf{D} + \alpha \mathbf{I}) \mathbf{P} e^{\alpha t}. \quad (39)$$

The approximation due to truncation already happens at this step. With these ingredients, the perturbation equation (6) can be expressed in terms of the truncated Fourier coefficients

$$\mathbf{U}(t)^T (\omega \mathbf{D} + \alpha \mathbf{I}) \mathbf{P} e^{\alpha t} = \mathbf{J}(t) \mathbf{U}(t)^T \mathbf{P} e^{\alpha t}. \quad (40)$$

The classical truncated Hill matrix equates the $2N + 1$ most centered Fourier coefficients of the periodic components of (40), which gives

$$\frac{1}{T} \int_0^T \mathbf{U}^* \mathbf{U}^T (\omega \mathbf{D} + \alpha \mathbf{I}) \mathbf{P} dt = \frac{1}{T} \int_0^T \mathbf{U}^* \mathbf{J}(t) \mathbf{U}^T \mathbf{P} dt \quad (41)$$

or, after elimination of identity matrices and shifting $\omega \mathbf{D}$ to the other side of the equation,

$$\alpha \mathbf{P} = (-\omega \mathbf{D} + \mathcal{F}(\mathbf{J}(t) \mathbf{U}^T)) \mathbf{P} = \mathbf{H} \mathbf{P}. \quad (42)$$

This is an eigenvalue problem for $\alpha, \mathbf{P}, \mathbf{H}$. In the limit $N \rightarrow \infty$, we recognize the classical eigenvalue problem of the Floquet forms of Section 2.2. This proves that the Jacobian matrix of the HBM equations \mathbf{H} indeed results from the classical Hill determinant procedure after truncation, justifying the name and symbol choice for \mathbf{H} .

4.2. Transformation between formulations

As the Hill matrices determined from different Fourier series orderings all have the same spectrum $\alpha_1, \dots, \alpha_n$, they must be related by similarity transform. Consider two matrices of Fourier basis functions $\mathbf{U}(t), \tilde{\mathbf{U}}(t)$ related by a constant transformation matrix $\tilde{\mathbf{U}}(t) = \mathbf{T}^T \mathbf{U}(t)$. The transformation matrix is introduced in a transposed form as $\mathbf{U}(t)^T$ is considered in the relevant applications. For example, $\mathbf{U}(t)$ could be the set of complex-valued Fourier basis functions and $\tilde{\mathbf{U}}$ a set of real-valued ones. For this case, all matrices are given explicitly in Appendix B.3. With

$$\begin{aligned} \mathbf{x}(t) &= \mathbf{U}(t)^T \mathbf{X} = (\mathbf{T}^{-T} \tilde{\mathbf{U}}(t))^T \mathbf{X} \\ &= \tilde{\mathbf{U}}(t)^T (\mathbf{T}^{-1} \mathbf{X}) = \tilde{\mathbf{U}}(t)^T \tilde{\mathbf{X}} \end{aligned} \quad (43)$$

we can infer the inverse transposed relationship for the Fourier coefficients $\tilde{\mathbf{X}} = \mathbf{T}^{-1} \mathbf{X}$. Although not generally true, the matrix \mathbf{T} may in practice often be orthogonal. In this case, the relationships for Fourier basis and Fourier coefficients coincide. The relationship between Fourier coefficients also holds for the HBM residual

$$\tilde{\mathbf{R}}(\tilde{\mathbf{X}}) = \mathbf{T}^{-1} \mathbf{R}(\mathbf{T} \tilde{\mathbf{X}}). \quad (44)$$

Assuming that the Hill matrix $\mathbf{H} = \frac{\partial \mathbf{R}(\mathbf{X})}{\partial \mathbf{X}}$ in one Fourier basis is known, the Hill matrix in the other Fourier basis can then be calculated using the chain rule

$$\tilde{\mathbf{H}} = \frac{\partial \tilde{\mathbf{R}}(\tilde{\mathbf{X}})}{\partial \tilde{\mathbf{X}}} = \mathbf{T}^{-1} \frac{\partial \mathbf{R}}{\partial \mathbf{X}} \mathbf{T} = \mathbf{T}^{-1} \mathbf{H} \mathbf{T}, \quad (45)$$

confirming the similarity relationships between the Hill matrices for different Fourier series representations and providing the transformation matrix explicitly.

4.3. Koopman–Hill projection for the real-valued Hill matrix

With the results of the previous section, the Koopman–Hill projection stability method extends easily to other Fourier series representations without needing to repeat the proof of [12] as the similarity transform (45) relates any generalized Hill matrix directly to the complex-valued Hill matrix. Denote by \mathbf{H}_{cplx} the classical Hill matrix obtained from the complex-valued Fourier series representation. An approximation of the monodromy matrix is given by $\mathbf{C} e^{\mathbf{H}_{\text{cplx}} T} \mathbf{W}$, as introduced in Section 2.3. Any Hill matrix $\tilde{\mathbf{H}}$ of a different Fourier series representation is related to \mathbf{H}_{cplx} by similarity $\mathbf{H}_{\text{cplx}} = \mathbf{T} \tilde{\mathbf{H}} \mathbf{T}^{-1}$, where \mathbf{T} only depends on the relationships between the Fourier bases, so \mathbf{T} and \mathbf{T}^{-1} can be determined once-and-for-all. This similarity transform can be substituted into the matrix exponential of the monodromy matrix estimate (14) to yield

$$\Phi_T \approx \mathbf{C} \mathbf{T} e^{\tilde{\mathbf{H}} T} \mathbf{T}^{-1} \mathbf{W}. \quad (46)$$

The matrices $\tilde{\mathbf{C}} := \mathbf{C} \mathbf{T}$ and $\tilde{\mathbf{W}} := \mathbf{T}^{-1} \mathbf{W}$ are problem-independent and can also be determined once-and-for-all at the start of computations.

For instance, if the Fourier coefficients are sorted as in Appendix B, the projection matrices become

$$\tilde{\mathbf{C}} = \mathbf{C} \mathbf{T} = (\mathbf{I} \quad \mathbf{0} \quad \dots \quad \mathbf{0}) \quad (47a)$$

$$\tilde{\mathbf{W}} = (\mathbf{I} \quad 2\mathbf{I} \quad \dots \quad 2\mathbf{I} \quad \mathbf{0} \quad \dots \quad \mathbf{0}) \quad (47b)$$

with $\tilde{\mathbf{W}}$ being constructed from N repeating blocks each reading $2\mathbf{I}$ and $\mathbf{0}$, respectively. This makes the Koopman–Hill projection approach easily applicable to Hill matrices for any Fourier basis with the same structural properties as for the classical complex matrix. Numerically, the cost of evaluating the matrix exponential of a real-valued matrix is generally less than a complex-valued one of the same dimension, so the real-valued formulation (46), (47a) is more efficient than the classical complex-valued form in application.

5. Examples

In this section, the computational performance of the Koopman–Hill projection stability method together with the differential quadratic recast is illustrated using a reduced-order model (ROM) of a nonlinear bending beam with hinged-hinged and clamped-clamped boundary conditions.

We consider two benchmark examples of a nonlinear von Kármán bending beam that is periodically forced. The beam has a length L , a cross-section of constant area A and second moment of area I , and is made of a homogeneous isotropic material with density ρ , and Young's modulus E . An Euler–Bernoulli kinematics is considered, the axial and rotatory inertia are neglected and the nonlinear strain is modeled using the usual von Kármán assumptions [53]. The two situations sketched in Fig. 5 are considered: a hinged-hinged beam with two point forces in phase opposition with frequency close to the one of the first bending resonance, as considered in [9,53,54], and a clamped-clamped beam with a single point harmonic force in the vicinity of the second bending resonance, considered in [51,55,56]. Fig. 5 also shows the corresponding linear mode shapes.

By denoting the transverse displacement field of the beam by $w(x, t)$ at time t and location x on the middle line, the partial differential equations of motion read

$$\rho A w_{,tt} + E I w_{,xxxx} - N w_{,xx} = p, \quad (48a)$$

$$N = \frac{E A}{2 L} \int_0^L w_{,x}^2 dx, \quad (48b)$$

where $N(t)$ is the axial force independent of x that is nonlinearly created by the large transverse displacement due to the immovable ends in the axial direction at $x = 0$ and $x = L$, and $p(x, t)$ is an external force per unit length.

Considering h to be the thickness of the cross-section and using the following dimensionless quantities, denoted by an overbar,

$$\begin{aligned} \bar{x} &= \frac{x}{L}, \quad \bar{w} = \frac{w}{h}, \quad \bar{t} = \frac{1}{L^2} \sqrt{\frac{E I}{\rho A}} t, \\ \bar{N} &= \frac{L^2}{h^2 E A} N, \quad \bar{p} = \frac{L^4}{h E I} p \end{aligned} \quad (49)$$

yields the dimensionless von Kármán PDE

$$\bar{w}_{,\bar{t}\bar{t}} + \bar{w}_{,\bar{x}\bar{x}\bar{x}\bar{x}} - \epsilon \bar{N} \bar{w}_{,\bar{x}\bar{x}} = \bar{p}, \quad (50a)$$

$$\bar{N} = \frac{1}{2} \int_0^1 \bar{w}_{,\bar{x}}^2 d\bar{x}, \quad (50b)$$

with the factor $\epsilon = h^2 A / I$ that depends only on the geometry of the cross-section. In the case of a rectangular shape, considered in the following, $\epsilon = 12$. It is convenient to define the radius of gyration of the cross section $r = \sqrt{I / A}$, which is $r = h / \sqrt{12}$ in the case of a rectangular cross-section.

Using the modal expansion

$$\bar{w}(\bar{x}, \bar{t}) = \sum_{j=1}^K q_j(\bar{t}) \phi_j(\bar{x}), \quad (51)$$

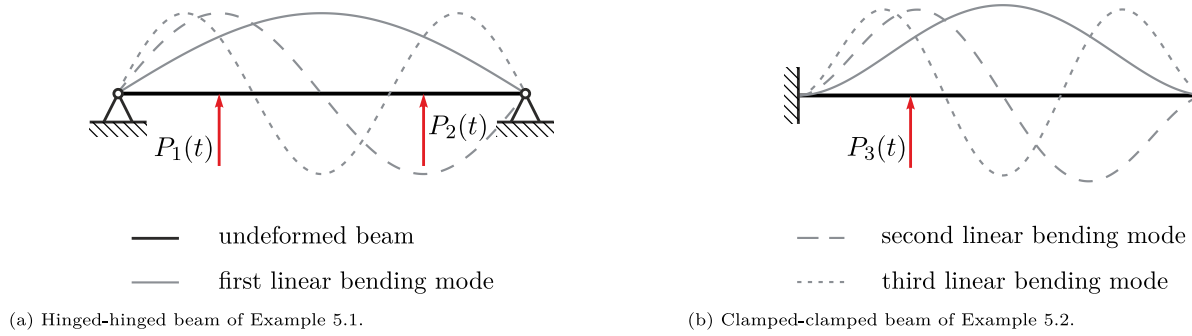


Fig. 5. Illustration of beam configurations and their linear modes.

where ϕ_j is the j th eigenmode shape of the beam, normalized such that $\int_0^1 \phi_j^2(\bar{x}) d\bar{x} = 1 \forall j$, the nonlinear PDE (50) can be approximated by the problem [54,56]

$$\ddot{q}_j + 2\xi_j \omega_j \dot{q}_j + \omega_j^2 q_j + \epsilon \bar{N} \sum_{i=1}^K h_{ij} q_i = Q_j, \quad j = 1, \dots, K \quad (52a)$$

$$\bar{N} = \frac{1}{2} \sum_{i=1}^K \sum_{j=1}^K h_{ij} q_i q_j, \quad (52b)$$

where a linear modal viscous damping term with damping factor ξ_j has been introduced. The factors h_{ij} and the modal forcing $Q_j(t)$ are given by

$$h_{ij} = \int_0^1 \phi_i'(\bar{x}) \phi_j'(\bar{x}) d\bar{x}, \quad Q_j(t) = \int_0^1 \phi_j(\bar{x}) \bar{p}(\bar{x}, \bar{t}) d\bar{x} \quad (53)$$

after projection onto the modal expansion.

5.1. Hinged-hinged von Kármán beam

For the hinged-hinged boundary conditions, the j th dimensionless eigenfrequency, normalized eigenmode shape and nonlinear coefficient h_{ij} are given in closed form by

$$\omega_j = \pi^2 j^2, \quad \phi_j(x) = \sqrt{2} \sin(j\pi x) \quad (54a)$$

$$h_{jj} = \omega_j, \quad h_{ij} = 0, \quad \forall i \neq j. \quad (54b)$$

The system (52) is already in the form of a DAE with algebraic quadratic nonlinearities and is also in the form (31), which permits an efficient differential quadratic recast with auxiliary variable $z = 2\bar{N}$. The beam is driven by two harmonic point forces $P_1(t)$ and $P_2(t)$ in phase opposition, applied at $\bar{x}_1 = 0.25$ and $\bar{x}_2 = 0.75$, respectively. This leads to

$$\bar{p}(\bar{x}, t) = \bar{P}_1(t) \delta(\bar{x} - \bar{x}_1) + \bar{P}_2(t) \delta(\bar{x} - \bar{x}_2), \quad (55)$$

such that $Q_j(t) = \bar{P}_1(t) \phi_j(\bar{x}_1) + \bar{P}_2(t) \phi_j(\bar{x}_2)$, where \bar{P}_1, \bar{P}_2 are the dimensionless forces.

To obtain the differential recast, we introduce an error $e = z - \sum_{j=1}^K \omega_j q_j^2$ for the corresponding equation (52b). With the postulated error dynamics $\dot{e} = -ke$, $k > 0$, and with the value of h_{ij} of Eq. (54b), the differential quadratic recast becomes

$$\dot{q}_j = u_j, \quad j = 1, \dots, K \quad (56a)$$

$$\dot{u}_j = -2\xi_j \omega_j u_j - \omega_j^2 q_j - 6\omega_j z q_j + Q_j, \quad j = 1, \dots, K \quad (56b)$$

$$\dot{z} = -k \left(z - \sum_{j=1}^K \omega_j q_j^2 \right) + 2 \sum_{j=1}^K \omega_j q_j u_j. \quad (56c)$$

This system of $n = 2K + 1$ quadratic ordinary differential equations is used for the investigations below. With respect to stability, we expect one additional Floquet exponent at $-k$ due to the differential recast. A value of $k = 50$ is chosen in the computations below. The parameters

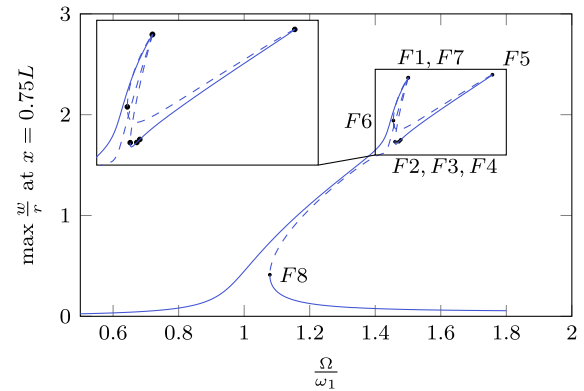


Fig. 6. Frequency response curve (maximal amplitude of $u(x,t)$ at $x = 0.75L$) of the hinged-hinged beam around its first bending resonance computed with $K = 10, N = 16$. Solid lines denote stable, and dashed lines denote unstable branches. Bifurcation points are labeled $F1, \dots, F8$.

Table 1

Parameters for the two beam benchmarks of Section 5.

ξ_j	$\bar{P}_1(t)$	$\bar{P}_2(t)$	$\bar{P}_3(t)$
$0.005 \frac{m}{\omega_j}$	$-13.63 \cos \Omega t$	$9.62 \cos \Omega t$	$18 \cos \Omega t$

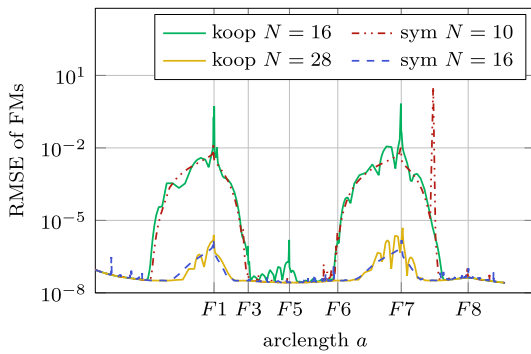
used in this work are given in Table 1, where $P_{1,2,3}(t)$ are already given in normalized units.

The frequency response of the hinged-hinged beam with the given parameters is known to exhibit a 1:3 internal resonance on the first mode [54,56]. The frequency response diagram obtained using the differential recast with $K = 10, H = 16$ given in Fig. 6 clearly shows this resonance, agreeing well with the literature results [9,53,54]. Fig. 6 displays the transverse displacement normalized by the radius of gyration $r = \sqrt{\frac{I}{bh}}$ instead of the height h to conform in scaling to the examples in literature.

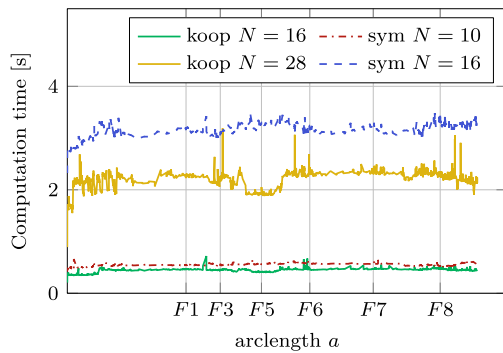
According to Fig. 6, the frequency response curve experiences fold bifurcations at $F1, F2, F5, F6, F7, F8$ and Neimark-Sacker bifurcations at $F3, F4$. This leads to bistable and even tristable regions.

Fig. 7 compares the computational effort and accuracy for the stability computation for the parameters of Fig. 6, but with different Hill matrix truncation orders and stability approaches. As the FRC of Fig. 6 folds on itself, every point on the branch is uniquely addressed by its arclength value instead of its frequency Ω in Fig. 7. The arclengths of the bifurcation points $F1, \dots, F8$ are given as reference.

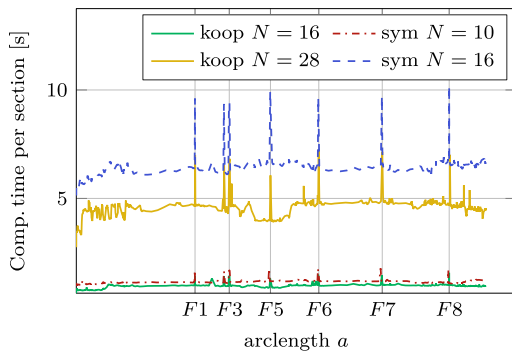
For every sample point on the FRC branch, Fig. 7(a) shows the minimal root mean square error (RMSE) between Floquet multipliers (FMs) computed from the Hill matrix using the Koopman projection method of Section 2.3 (“koop”) or the symmetry-based eigenvalue sorting method [9] (“sym”) that is implemented by default in MANLAB, version 4.1.7 [44], and reference FMs that were computed in the time



(a) RMS error of Floquet multipliers for different stability methods along the arclength of the FRC.



(b) Computation time per stability computation for different stability methods along the arclength of the FRC.



(c) Computation time per section for different stability methods along the arclength of the FRC.

Fig. 7. RMS error of Floquet multipliers and computation time along the arclength of the branch for different approaches and different truncation orders.

domain using a variable-step single pass method based on the fixed-step method reported in [6, Section 3.1.3], but using Matlab's ode45 solver. The chosen absolute and relative tolerances provide the FMs with accuracy of approximately 10^{-8} . Fig. 7(b) shows the computation time that was needed exclusively for stability computation, i.e., to produce these Floquet multipliers from the Hill matrix using the respective methods and truncation orders. Fig. 7(c) shows the overall computation time that was needed to compute a given section of the branch, constituted by the time to solve the HBM problem via ANM and two stability determinations at the start and end of the section, respectively. Around bifurcation points, additional stability computations are executed to find the exact bifurcation point. For all approaches, the computation time of the HBM problem is insignificant compared to the computation time of the stability determination.

The RMSE of all methods at all truncation orders is highest around the bifurcation points $F1$ and $F7$ corresponding to the 1:3 internal resonance. This is expected as, at these points, the frequency contribution of higher frequencies is strong, amplifying errors due to truncation. For the symmetry-based method, a satisfactory accuracy where stability is always asserted correctly is achieved at a truncation order $N = 10$ of the Hill matrix. There is one outlier between bifurcations $F7$ and $F8$, where the symmetry-based sorting criterion does not correctly identify all Floquet exponents, selecting two Floquet exponents of the same group and missing another group completely.

The Koopman projection method as is known to be less accurate than the symmetry-based method for fixed truncation order [12]. This is reflected in Fig. 7(a) as (roughly) the same RMSE is only achieved at $N = 16$. However, due to the superior computational efficiency, the computation time for the Koopman projection method for $N = 16$ with less than 0.5 s on average is still lower than that of the symmetry-based method at $N = 10$. This also means that, with similar overall computation time, the branch can be tracked by a more exact HBM of higher truncation order if Koopman–Hill projection is employed. If a higher accuracy of Floquet multipliers is desired, the truncation order must be increased. A truncation order of $N = 16$ for the symmetry-based method and of $N = 28$ for the Koopman projection method yield a comparable accuracy of approximately 10^{-6} at the bifurcation points $F1, F7$. Again, the computation time of the symmetry-based method with $N = 16$ is approximately 50% higher per step than that of the Koopman projection method with $N = 28$.

5.2. Clamped-clamped beam

In this section, the PDE (50) is considered with clamped-clamped boundary conditions, where the eigenmodes cannot be given in fully closed form. The linear eigenfrequencies $\omega_k = \beta_k^2$ fulfill the transcendental equation $\cos \beta_k \cosh \beta_k = 1$, with $\beta_k \approx (2k + 1)/\pi$ for $k > 3$ [57] and the corresponding eigenmodes are given before normalization by

$$\begin{aligned} \phi_k(x) = & (\sin \beta_k - \sinh \beta_k) (\cos \beta_k x - \cosh \beta_k x) \\ & - (\cos \beta_k - \cosh \beta_k) (\sin \beta_k x - \sinh \beta_k x). \end{aligned} \quad (57)$$

The first three eigenmodes are visualized in Fig. 5(b). Substitution of this modal decomposition into (48) yields the modal expansion (52), in which the factors h_{ij} must be determined numerically using equation (53)a. In the benchmark considered here, the beam is driven by a harmonic point force $P_3(t)$ applied at $\bar{x}_3 = 0.275$, leading to $Q_j(t) = \phi_j(\bar{x}_3) \bar{P}_3(t)$.

In contrast to the hinged-hinged case, the non-vanishing factors h_{ij} cause more coupling between states, leading to a more densely populated Jacobian matrix of the linearization. The FRF curve of Fig. 8 shows that the first resonance has a bistable region and admits two fold bifurcations $F1, F2$. One can notice that the particular rounded top of the resonance curve is due to a 1:3 internal resonance between bending mode 2 and 4 of the beam [51].

In Fig. 9, the computation time for the Floquet multipliers with different methods as well as their RMSE against a reference solution using a single pass method of accuracy 10^{-8} are given. Compared to the hinged-hinged case, higher truncation orders are needed to arrive at the same RMSE of Floquet multipliers for all approaches. This can be attributed to the more coupled structure of the equations. As in the hinged-hinged case, the Koopman projection method requires higher truncation orders than the symmetry-based method to arrive at approximately the same RMSE values. Even more significantly than in the hinged-hinged case, however, the Koopman projection method is roughly 30% – 50% faster despite the increased truncation order.

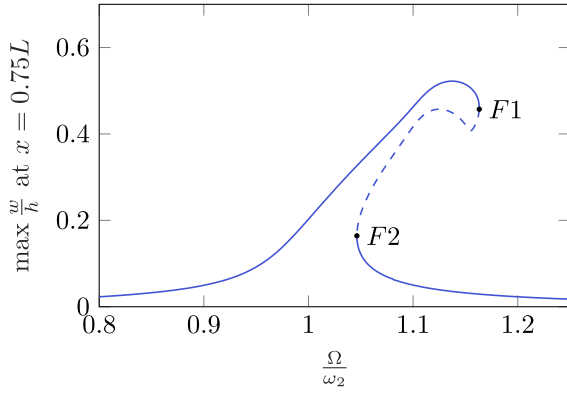
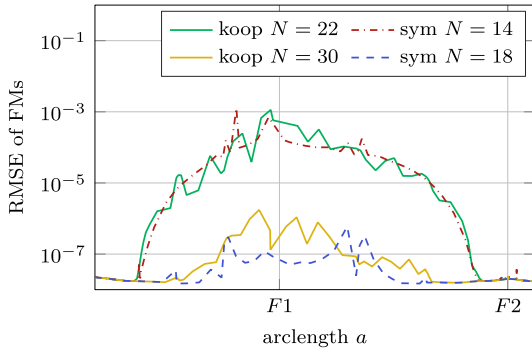
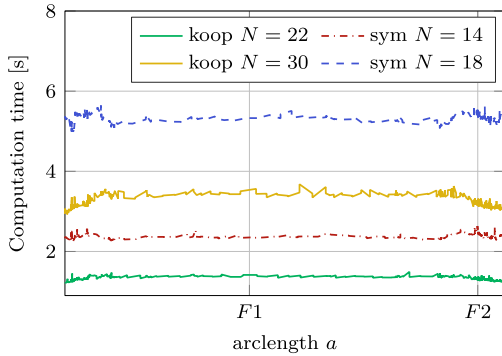


Fig. 8. Frequency response curve (maximal amplitude of $\frac{w(x,t)}{h}$ at $x = 0.75L$) of the clamped-clamped beam around its second bending resonance computed with $K = 5, N = 20$. Solid lines denote stable, dashed lines denote unstable branches. Bifurcation points are labeled by $F1, F2$.



(a) RMS error of Floquet multipliers for different stability methods along the arclength of the FRC.



(b) Computation time per stability computation for different stability methods along the arclength of the FRC.

Fig. 9. RMS error of Floquet multipliers and computation time along the arclength of the branch for different approaches and different truncation orders.

5.3. An observation for a lift with subharmonic frequencies

The choice of how to go back from lifted coordinates $\mathbf{z} \in \mathbb{C}^{n(2N+1)}$ to original coordinates $\mathbf{y} \in \mathbb{R}^n$ is not unique. Instead of using only the middle entry \mathbf{z}_0 , other linear combinations of the \mathbf{z}_k in (13) given by

$$\mathbf{C}(t)\mathbf{z}(t) := \sum_{k=-N}^N c_k e^{ik\omega t} \mathbf{z}_k(t) \approx \sum_{k=-N}^N c_k \mathbf{y}(t) \quad (58)$$

also yield \mathbf{y} as an approximate result if the sum of all c_k is one and the columns of $\mathbf{C}(t)$ are additionally adjusted by terms of the form $e^{ik\omega t}$. An optimization approach involving a quadratic program was

proposed in [12] to systematically find values for the c_k that ensure high accuracy of the monodromy matrix. For the hinged-hinged and the clamped-clamped beam as considered in the previous sections, the optimal solution is indeed very close to the naive projection presented in Section 2.3 that only returns \mathbf{z}_0 and discards contributions of all other elements. Further numerical studies by the authors suggest that this is generally the case for most system formulations, independent of the type of nonlinearity.

However, if the Hill matrix is constructed in the subharmonic fashion described below, the optimal solution for the coefficients c_k differs. If \mathbf{J} is periodic with period T , then it is periodic with period $2T$ as well, meaning that it can also be expressed by the Fourier series

$$\mathbf{J}(t) = \sum_{k=-\infty}^{\infty} \mathbf{J}_k e^{i\frac{k}{2}\omega t} \quad (59)$$

of base frequency $\frac{\omega}{2}$, where $\mathbf{J}_{\frac{k}{2}}$ is zero if $\frac{k}{2} \notin \mathbb{Z}$. Considering the frequency $\frac{\omega}{2}$ allows to construct a subharmonic Hill matrix of twice the size as the classical Hill matrix, where every second block entry is zero and which still contains the same Fourier coefficients $\mathbf{J}_{-2N}, \dots, \mathbf{J}_{2N}$. As the subharmonic Hill matrix is in $\mathbb{C}^{n(4N+1) \times n(4N+1)}$, the corresponding state $\mathbf{z} \in \mathbb{C}^{n(4N+1)}$ of the Koopman lift (13) is partitioned as $\mathbf{z}^T = (\mathbf{z}_{-N}^T, \mathbf{z}_{-2N+1}^T, \dots, \mathbf{z}_N^T)$.

For this subharmonic Hill matrix and the hinged-hinged beam example, the optimization procedure of [12] yields instead of the naive projection $\mathbf{y}(t) = \mathbf{z}_0(t)$ the more sophisticated projection

$$\mathbf{y}(t) \approx \mathbf{C}_{\text{subh}}(t)\mathbf{z}(t) = \sum_{k=-2N}^{2N} (-1)^k e^{i\frac{k}{2}\omega t} \mathbf{z}_{\frac{k}{2}}(t). \quad (60)$$

This is consistent with the results of [12], where the Mathieu-equation-based examples were incidentally constructed in such a subharmonic fashion. Evaluated after one (original) period of the system, the exponential terms exactly cancel the alternating factors and this yields for the monodromy matrix the expression

$$\Phi_T \approx \mathbf{C}_{\text{subh}}(T) e^{\mathbf{H}_{\text{subh}} T} \mathbf{W}_{\text{subh}} \quad (61)$$

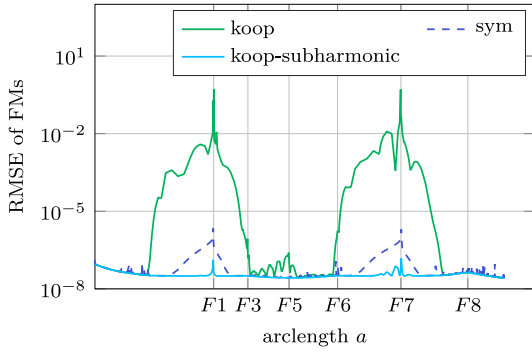
with

$$\mathbf{C}_{\text{subh}}(T) = \mathbf{W}_{\text{subh}}^T = (\mathbf{I}, \dots, \mathbf{I}). \quad (62)$$

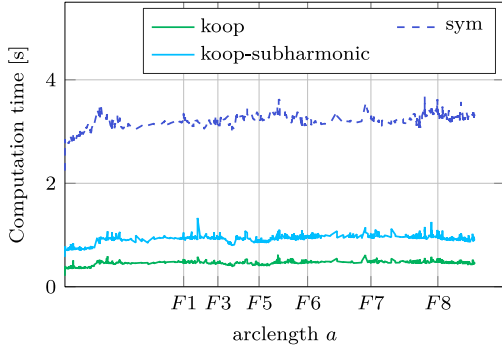
Essentially, the subharmonics-based approximation encodes the naive approximation (14) as above, with an additive ‘‘correction’’ term due to the lifted states $\mathbf{z}_{\frac{k}{2}}$.

Due to the many zeros in the subharmonic Hill matrix of size $n(4N+1)$, a re-ordering of rows and columns brings it into a block-diagonal form with two blocks of sizes $n(2N+1)$ and $2nN$. This allows to evaluate two matrix exponentials of the two decoupled submatrices of (at most) the size of the original Hill matrix instead of one matrix exponential of twice the size. For fixed N , computing the monodromy matrix from the subharmonic Hill matrix by subharmonic projection is thus twice as costly as naive projection. As the decoupled structure persists also for a real-valued subharmonic Fourier series, this subharmonic approach can be constructed both in the complex-valued and in the real-valued case.

Fig. 10 shows the computation times and the RMSE of the Floquet multipliers of the hinged-hinged beam example with $K = 10$ and $N = 16$ for the standard Koopman projection and the symmetry-based eigenvalue sorting method (cf. Fig. 7), and additionally for the Koopman projection using the subharmonic Hill matrix and the heuristically determined projection (61), evaluated using two matrix exponentials per step. As expected, the computation time for the Koopman projection with the subharmonics-based modification is almost exactly twice as high as for the Koopman projection approach as two matrix exponentials need to be evaluated instead of one. The accuracy, however, is significantly improved by the use of the subharmonic structure. It is even better than that of the symmetry-based eigenvalue sorting method, which is much slower to compute.



(a) RMS error of Floquet multipliers for different stability methods along the arclength of the FRC.



(b) Computation time per stability computation for different stability methods along the arclength of the FRC.

Fig. 10. RMS error of Floquet multipliers and computation time along the arclength of the branch for different approaches with truncation order $N = 16$.

6. Conclusion

In this work, we showed that the truncated Hill matrix can be interpreted in three ways, independent of the choice of real or complex-valued Fourier series: firstly, as the truncation of the infinite Hill determinant problem; secondly, as the Jacobian of the HBM problem; and finally, as the constant system matrix of a higher-dimensional lifted linear system. For quadratic ODEs obtained by the differential recast proposed in this work, the combination of these three properties allows to extract and use the Hill matrix for stability determination immediately during an ANM continuation procedure, without any additional condensation steps.

As a novel result applicable to any HBM continuation framework, we generalized the sparsity-exploiting Koopman projection stability approach to real-valued Hill matrix formulations. In conjunction with ANM, we showed that it reduces the computation time for stability determination of the HBM solution compared to classical Hill methods, which rely on finding the complete eigendecomposition of the Hill matrix. In its standard variant, this projection approach requires higher truncation orders for the same Floquet multiplier accuracy, still retaining lower overall computation time per step regardless.

We also observed in this work that the accuracy of the Koopman projection stability method can be improved by a special, subharmonic choice of projection matrix. Numerical studies for other systems indicate that this subharmonic method universally improves accuracy. However, further research is needed to provide guarantees for arbitrary classes of systems.

With broader applications in mind, the differential recast approach could be extended to other cases of nonlinearities that the ANM and Manlab are in principle able to deal with, to bring the immediate availability of the Hill matrix to other types of systems such as multibody

systems or large finite element geometrically exact beam models that include unitary quaternions. In addition, thorough numerical studies that compare the performance of the Koopman–Hill method to other stability methods especially at very large system sizes could give important insight for practical applications. The particular case of marginally stable periodic solutions encountered in the computation of the backbone curves of nonlinear modes is a straightforward application of the present work, whose exemplification is also left for further studies.

CRedit authorship contribution statement

Fabia Bayer: Writing – original draft, Software, Methodology, Investigation, Formal analysis, Conceptualization. **Remco I. Leine:** Writing – review & editing, Supervision, Project administration, Methodology, Investigation, Conceptualization. **Olivier Thomas:** Writing – review & editing, Methodology, Conceptualization. **Aurélien Grolet:** Writing – review & editing.

Declaration of competing interest

The authors declare that they have no known competing financial interests or personal relationships that could have appeared to influence the work reported in this paper.

Data availability

Data will be made available on request.

Appendix A. Convergence proof for the differential recast

A.1. Periodic solutions of differential recast

In this section, we will prove that any periodic solutions of the differential quadratic recast (30) are of the form $z_\beta^p(t) = \mathbf{x}^p(t)^\beta$, where $\mathbf{x}^p(t)$ is a periodic solution of the original polynomial dynamics (27). We denote the j th entry of \mathbf{f} by f_j and of \mathbf{h}_β by $h_{\beta,j}$. To prove the anticipated stability properties, we transform the differential recast (30) from auxiliary coordinates (\mathbf{x}, \mathbf{z}) into error coordinates (\mathbf{x}, \mathbf{e}) using the relation (28). With the chain rule, differentiation of (28) yields

$$\dot{e}_\beta = \dot{z}_\beta - \sum_{j=1}^n \beta_j \mathbf{x}^{\beta-e_j} \dot{x}_j. \quad (63)$$

Subsequently, every occurrence of z_β in $(\dot{\mathbf{x}}, \dot{\mathbf{e}})$ is substituted by $z_\beta = e_\beta + \mathbf{x}^\beta$ to yield the error dynamics

$$\dot{x}_j = f_j(\mathbf{x}, t) + \sum_{2 \leq |\beta| \leq m} h_{\beta,j} e_\beta, \quad 1 \leq j \leq n_b \quad (64a)$$

$$\dot{e}_\beta = -k e_\beta, \quad |\beta| = 2 \quad (64b)$$

$$\dot{e}_\beta = -k \left(e_\beta - x_l e_{\beta-e_l} \right) + \sum_{j=1}^n \beta_j \left(f_j(\mathbf{x}, t) + \sum_{2 \leq |\gamma| \leq m} h_{\gamma,j} e_\gamma \right) e_{\beta-e_j}, \quad 3 \leq |\beta| \leq m. \quad (64c)$$

Eqs. (64a) and (64b) follow directly from substitution. For (64c), the relation $z_\beta = e_\beta + \mathbf{x}^\beta$ has been used to eliminate z_β , re-identifying $f_j(\mathbf{x}, t)$ in $\tilde{f}_j(\mathbf{x}, \mathbf{x}^{\beta(1)} + e_{\beta(1)}, \dots, \mathbf{x}^{\beta(M)} + e_{\beta(M)}, t)$. The error dynamics of order $|\beta| = 2$ in (64b) consists of n_b decoupled scalar linear differential equations with a globally asymptotically stable equilibrium at $e_\beta = 0$. This means that all stationary solutions of (64) must fulfill $e_\beta \equiv 0$ for $|\beta| = 2$.

The error dynamics for higher orders is given by (64c). Except for a proportional term $-k e_\beta$, every summand of (64c) is multiplied by an error coordinate of lower order than $|\beta|$. As e_β with $|\beta| = 2$ must vanish for any stationary solution, (64c) for $|\beta| = 3$ on the stationary solution becomes again decoupled with a globally asymptotically stable

equilibrium at the origin being the only stationary solution. This induction process can be completed order by order to yield $e_\beta \equiv 0$ on any stationary solution for all β with $|\beta| \geq 2$. Equivalently, the differential quadratic recast must fulfill $z_\beta = \mathbf{x}^\beta$ on any stationary solution. If $e_\beta \equiv \mathbf{0}$, then (64a) reduces to the original dynamics. Therefore, stationary solutions of the differential recast and the original system coincide.

A.2. Floquet exponents of differential recast

The lower triangular structure of the error dynamics (64) which decouples at a stationary solution with $e_\beta \equiv 0$ suggests that every row of the error dynamics adds an additional Floquet exponent at $-k$. In this section, we show that this is indeed the case.

To analyze the Floquet quantities, we construct the principal fundamental solution matrix in semi-closed form. As shown in Appendix A.1, stationary and, in particular, periodic solutions $(\mathbf{x}^p(t), e^p(t))$ of (64) always fulfill $e^p \equiv \mathbf{0}$, hence \mathbf{x}^p must be a stationary solution of the original dynamics (27). Evaluating the Jacobian (6) of (64) around a periodic solution of this structure, the perturbation equation is given by

$$\begin{pmatrix} \Delta \dot{\mathbf{x}} \\ \Delta \dot{e} \end{pmatrix} = \begin{pmatrix} \frac{\partial f}{\partial \mathbf{x}} \Big|_{\mathbf{x}^p(t)} & \begin{pmatrix} \mathbf{h}_{\beta^{(1)}} & \dots & \mathbf{h}_{\beta^{(M)}} \end{pmatrix} \\ \mathbf{0} & \mathbf{K}(t) \end{pmatrix} \begin{pmatrix} \Delta \mathbf{x} \\ \Delta e \end{pmatrix} \quad (65)$$

where $\mathbf{K}(t)$ is a lower triangular matrix with $-k$ as its diagonal entries and terms linear in \mathbf{x} or of the form $f_j(\mathbf{x}^p(t), t)$ below the diagonal. In particular, as (65) is evaluated for a periodic solution, $\mathbf{K}(t)$ itself is also T -periodic.

It is immediately clear that the dynamics $\Delta \dot{e} = \mathbf{K}(t)\Delta e$ in the lower blocks is decoupled from the $\Delta \mathbf{x}$ -dynamics. Due to the triangular structure of \mathbf{K} , we can solve the lower rows in semi-closed form using induction, finding asymptotically autonomous [58] structure in the error dynamics. The first row of the lower block, corresponding to (64b), reads $\Delta \dot{e}_{\beta^{(1)}} = -k\Delta e_{\beta^{(1)}}$, which can be immediately solved to

$$\Delta e_{\beta^{(1)}}(t) = e^{-kt} \Delta e_{\beta^{(1)}}(0) \quad (66)$$

for arbitrary initial conditions $\Delta e_{\beta^{(1)}}(0)$. As induction assumption, we require that the first $l - 1$ solutions of the lower block are given in Floquet form

$$\Delta e_{\beta^{(i)}}(t) = p_i(t, \Delta e(0)) e^{-kt} \quad 1 \leq i \leq l - 1 \quad (67)$$

with $p_i(t, \Delta e) = p_i(t + T, \Delta e)$ a T -periodic function that depends on the arbitrary initial condition $\Delta e(0)$. This is trivially satisfied for $l = 2$ by (66) with $p_1(t, \Delta e) = \Delta e_{\beta^{(1)}}(0)$, independent of t . We can express the differential equation for the l th solution of the lower block in terms of the solutions with known structure

$$\Delta \dot{e}_{\beta^{(l)}}(t) = -k\Delta e_{\beta^{(l)}}(t) + \sum_{i=1}^{l-1} K_{li}(t)p_i(t)e^{-kt}, \quad (68)$$

which is a scalar linear inhomogeneous differential equation with homogeneous solution

$$\Delta e_{\beta^{(l)}}_{\text{hom}}(t) = \Delta e_{\beta^{(l)}}(0) e^{-kt} \quad (69)$$

and particular solution

$$\Delta e_{\beta^{(l)}}_{\text{part}}(t) = e^{-kt} \int_0^t \sum_{i=1}^{l-1} K_{li}(\tau)p_i(\tau)d\tau, \quad (70)$$

yielding the solution

$$\begin{aligned} \Delta e_{\beta^{(l)}}(t) &= e^{-kt} \left(\Delta e_{\beta^{(l)}}(0) + \int_0^t \sum_{i=1}^{l-1} K_{li}(\tau)p_i(\tau)d\tau \right) \\ &=: p_l(t, \Delta e(0)) e^{-kt}, \end{aligned} \quad (71)$$

which is of the form (67) and thus completes the induction.

This means that also the lower right block of the fundamental solution matrix of (65) is constituted by a Floquet type solution $\mathbf{P}_e(t) e^{-kt}$

as it consists of columns of the form (67) for one specific initial condition. Conversely, due to the decoupled structure, it holds that $\Delta e \equiv \mathbf{0}$ for all $t \geq 0$ if $\Delta e(0) = 0$, recovering in the upper left block of the fundamental solution matrix of (64) the fundamental solution matrix $\Phi_{\text{nonl}}(t) = \mathbf{P}_x(t) e^{\mathbf{Q}_x t}$ of the periodic solution of the original nonlinear dynamics (27). In summary, the fundamental solution matrix is constituted by

$$\Phi(t) = \begin{pmatrix} \mathbf{P}_x(t) e^{\mathbf{Q}_x t} & * \\ \mathbf{0} & \mathbf{P}_e(t) e^{-kt} \end{pmatrix}, \quad (72)$$

which can be decoupled due to the block triangular structure into

$$\Phi(t) = \mathbf{P}(t) e^{\mathbf{Q}t} \quad (73a)$$

with

$$\mathbf{P}(t) = \mathbf{P}(t + T) = \begin{pmatrix} \mathbf{P}_x(t) & * \\ \mathbf{0} & \mathbf{P}_e(t) \end{pmatrix} \quad (73b)$$

$$\mathbf{Q} = \begin{pmatrix} \mathbf{Q}_x & * \\ \mathbf{0} & -k\mathbf{I} \end{pmatrix} \text{ constant} \quad (73c)$$

and $*$ denotes arbitrary terms of no further relevance. The Floquet exponents of the error dynamics (64) can be read off from (73c) due to its block-triangular structure to be the Floquet exponents of the original nonlinear dynamics (27) collected in \mathbf{Q}_x , and additional Floquet exponents at $-k$ for each row of the error dynamics. These Floquet exponents carry over to the differential quadratic recast (30).

Appendix B. Explicit Hill and transformation matrices for various Fourier bases

In Section 4, a linear transformation between representations for the Hill matrix has been derived. We will provide all involved quantities explicitly for two of the most commonly used basis choices:

1. the classical complex-valued basis

$$\mathbf{U}_{\text{cplx}}(t)^T := (e^{-iN\omega t} \quad \dots \quad e^{iN\omega t}) \otimes \mathbf{I}_{n \times n} \quad (74)$$

such that $\mathbf{x}(t) = \sum_{k=-N}^N \mathbf{x}_k e^{ik\omega t}$ with the coefficient vector $\mathbf{X}_{\text{cplx}}^T = (\mathbf{x}_{-N}^T, \dots, \mathbf{x}_N^T)$ and

2. a particular real-valued basis

$$\mathbf{U}_{\text{real}}(t) := \begin{pmatrix} 1 \\ \cos \omega t \\ \vdots \\ \cos N\omega t \\ \sin \omega t \\ \vdots \\ \sin N\omega t \end{pmatrix} \otimes \mathbf{I}_{n \times n} \quad (75)$$

such that $\mathbf{x}(t) = \sum_{k=0}^N \mathbf{a}_k \cos k\omega t + \mathbf{b}_k \sin k\omega t$ with $\mathbf{X}_{\text{real}}^T = (\mathbf{a}_0^T \quad \dots \quad \mathbf{a}_N^T \quad \mathbf{b}_1^T \quad \dots \quad \mathbf{b}_N^T)$.

B.1. Explicit expressions for complex Fourier series

With the well-known Fourier analysis equation [52]

$$\mathbf{x}_k = \frac{1}{T} \int_0^T \mathbf{x}(t) e^{-ik\omega t} dt, \quad (76)$$

the complex-valued Fourier analysis matrix $\mathbf{U}_{\text{cplx}}^*$ such that $\mathbf{X}_{\text{cplx}} = \frac{1}{T} \int_0^T \mathbf{U}_{\text{cplx}}^*(t) \mathbf{x}(t) dt$ is the complex conjugate of $\mathbf{U}_{\text{cplx}}(t)$

$$\mathbf{U}_{\text{cplx}}^*(t) = (e^{iN\omega t} \quad \dots \quad e^{-iN\omega t})^T \otimes \mathbf{I}_{n \times n}. \quad (77)$$

As the derivative $\frac{d}{dt} e^{ik\omega t} = ik\omega e^{ik\omega t}$ only depends on itself, the derivative matrix \mathbf{D}_{cplx} is given by a diagonal matrix

$$\begin{aligned} \dot{\mathbf{U}}_{\text{cplx}}(t)^T &= \mathbf{U}_{\text{cplx}}(t)^T \omega \mathbf{D}_{\text{cplx}} \\ &= \mathbf{U}_{\text{cplx}}(t)^T \omega i (\text{diag}\{-N, \dots, N\} \otimes \mathbf{I}_{n \times n}). \end{aligned} \quad (78)$$

To evaluate the complex-valued Hill matrix using (37), the Fourier coefficients of $\mathbf{J}(t)\mathbf{U}(t)^T$ must be determined. The Fourier series expansion of this matrix product is

$$\begin{aligned} \mathbf{J}(t)\mathbf{U}_{\text{cplx}}(t)^T &= \left(\sum_{k=-\infty}^{\infty} \mathbf{J}_k e^{i(k-N)\omega t} \quad \dots \quad \sum_{k=-\infty}^{\infty} \mathbf{J}_k e^{i(k+N)\omega t} \right) \\ &= \left(\sum_{k=-\infty}^{\infty} \mathbf{J}_{k+N} e^{ik\omega t} \quad \dots \quad \sum_{k=-\infty}^{\infty} \mathbf{J}_{k-N} e^{ik\omega t} \right). \end{aligned} \quad (79)$$

Reading off the Fourier coefficients from (79) and arranging them in block columns yields the complex-valued Hill matrix

$$\begin{aligned} \mathbf{H}_{\text{cplx}} &= -\omega \mathbf{D}_{\text{cplx}} + \mathcal{F}_N(\mathbf{J}(t)\mathbf{U}_{\text{cplx}}^T) \\ &= \begin{pmatrix} \mathbf{J}_0 + i\omega \mathbf{N}\mathbf{I} & \mathbf{J}_{-1} & \dots & \mathbf{J}_{-2N} \\ \mathbf{J}_1 & \mathbf{J}_0 + i\omega(N-1)\mathbf{I} & \dots & \mathbf{J}_{-2N+1} \\ \vdots & \vdots & \ddots & \vdots \\ \mathbf{J}_{2N} & \mathbf{J}_{2N-1} & \dots & \mathbf{J}_0 - i\omega \mathbf{N}\mathbf{I} \end{pmatrix}, \end{aligned} \quad (80)$$

which does indeed coincide with the expected expression (cf. Section 2.2, [10,22,28]).

B.2. Explicit expressions for real Fourier series

While there is an overwhelming consensus in the literature that the complex-valued basis is sorted in ascending order of frequency, there is no consensus on how to order the real-valued Fourier basis functions. The ordering presented here (first all cosines, then all sines) is often used [11,59], but also an alternating variant where cos and sin terms of the same frequency appear together is common [1,6,8,60–62]. We use the former variant here because it is also used to give an explicit construction formula for the real-valued Hill matrix in [11]. The transformation approach of Sections 4.2 and B.3 can be used to easily switch between orderings.

With $\mathbf{a}_0 = \frac{1}{T} \int_0^T \mathbf{x}(t) dt$, $\mathbf{a}_k = \frac{2}{T} \int_0^T \mathbf{x}(t) \cos k\omega t$, and $\mathbf{b}_k = \frac{2}{T} \int_0^T \mathbf{x}(t) \sin k\omega t$, the corresponding Fourier analysis matrix for \mathbf{U}_{real} is

$$\mathbf{U}_{\text{real}}^*(t) = \begin{pmatrix} 1 \\ 2 \cos \omega t \\ \vdots \\ 2 \cos N\omega t \\ 2 \sin \omega t \\ \vdots \\ 2 \sin N\omega t \end{pmatrix} \otimes \mathbf{I}_{n \times n}. \quad (81)$$

The derivative matrix \mathbf{D}_{real} is given by

$$\dot{\mathbf{U}}_{\text{real}}(t)^T = \mathbf{U}_{\text{real}}(t)^T \omega \mathbf{D}_{\text{real}} \quad (82)$$

with

$$\mathbf{D}_{\text{real}} = \begin{pmatrix} 0 & \mathbf{0}^T & \mathbf{0}^T \\ \mathbf{0} & \mathbf{0} & \text{diag}\{1, \dots, N\} \\ \mathbf{0} & -\text{diag}\{1, \dots, N\} & \mathbf{0} \end{pmatrix} \otimes \mathbf{I}_{n \times n}. \quad (83)$$

Again, the real-valued Hill matrix can be determined using (37). However, computing the Fourier coefficients of $\mathbf{J}(t)\mathbf{U}_{\text{real}}(t)$ requires the evaluation of trigonometric theorems and is significantly more involved than in the complex-valued case. After these algebraic calculations, the real-valued Hill matrix is

$$\mathbf{H}_{\text{real}} = -\omega \mathbf{D}_{\text{real}} + \begin{pmatrix} \mathbf{J}_c^{(0)} & \frac{1}{2} \mathbf{J}_c & \frac{1}{2} \mathbf{J}_s \\ \mathbf{J}_c^T & \mathbf{K}_c + \mathbf{T}_c & \mathbf{K}_s + \mathbf{T}_s \\ \mathbf{J}_s^T & \mathbf{K}_s - \mathbf{T}_s & \mathbf{T}_c - \mathbf{K}_c \end{pmatrix} \quad (84)$$

where we adapted the notation from [11, Appendix 3] for $\mathbf{J}(t) := \sum_{k=0}^{\infty} \mathbf{J}_c^{(k)} \cos k\omega t + \mathbf{J}_s^{(k)} \sin k\omega t$:

$$\mathbf{J}_{c,s} = \begin{pmatrix} \mathbf{J}_{c,s}^{(1)} & \dots & \mathbf{J}_{c,s}^{(N)} \end{pmatrix} \quad (85a)$$

$$\mathbf{K}_{c,s} = \frac{1}{2} \begin{pmatrix} \mathbf{J}_{c,s}^{(2)} & \mathbf{J}_{c,s}^{(3)} & \dots & \mathbf{J}_{c,s}^{(N+1)} \\ \mathbf{J}_{c,s}^{(3)} & \mathbf{J}_{c,s}^{(4)} & \dots & \mathbf{J}_{c,s}^{(N+2)} \\ \vdots & \vdots & \ddots & \vdots \\ \mathbf{J}_{c,s}^{(N+1)} & \mathbf{J}_{c,s}^{(N+2)} & \dots & \mathbf{J}_{c,s}^{(2N)} \end{pmatrix} \quad (85b)$$

$$\mathbf{T}_c = \frac{1}{2} \begin{pmatrix} 2\mathbf{J}_c^{(0)} & \mathbf{J}_c^{(1)} & \dots & \mathbf{J}_c^{(N-1)} \\ \mathbf{J}_c^{(1)} & 2\mathbf{J}_c^{(0)} & \dots & \mathbf{J}_c^{(N-2)} \\ \vdots & \vdots & \ddots & \vdots \\ \mathbf{J}_c^{(N-1)} & \mathbf{J}_c^{(N-2)} & \dots & 2\mathbf{J}_c^{(0)} \end{pmatrix} \quad (85c)$$

$$\mathbf{T}_s = \frac{1}{2} \begin{pmatrix} 0 & \mathbf{J}_s^{(1)} & \dots & \mathbf{J}_s^{(N-1)} \\ -\mathbf{J}_s^{(1)} & 0 & \dots & \mathbf{J}_s^{(N-2)} \\ \vdots & \vdots & \ddots & \vdots \\ -\mathbf{J}_s^{(N-1)} & -\mathbf{J}_s^{(N-2)} & \dots & 0 \end{pmatrix}. \quad (85d)$$

As in [11], the transposition $\mathbf{J}_{c,s}^T$ in (84) indicates block-wise transposition, i.e., the entries of each block $\mathbf{J}_{c,s}^{(k)}$ are *not* transposed. Compared to the literature result in [11, Eq. (28)], the sign of \mathbf{T}_s is flipped and the entries of the first row are halved. Numerical studies indicate that indeed (84) in conjunction with (85) is correct and does possess the same spectrum as \mathbf{H}_{cplx} , while we did not achieve consistent results using the formulation of [11, Eq. (28)].

As the explicit calculation of (84) is complicated and error-prone, it is easier in practice to obtain \mathbf{H}_{real} numerically as partial derivative of the HBM equations or using the similarity transformation of Section 4.2. However, the formulation (84) is necessary if the Fourier coefficients of the Jacobian matrix are sought or structural insight about the Hill matrix is needed.

B.3. Real to complex transformation matrices

To switch between real- and complex-valued representations, the transformation must be derived once and for all. With $e^{i\theta} = \cos \theta + i \sin \theta$, the transformation from real-valued to complex-valued basis functions is

$$\begin{aligned} \mathbf{U}_{\text{cplx}}(t) &:= \mathbf{T}^T \mathbf{U}_{\text{real}}(t) \\ &= \begin{pmatrix} \begin{pmatrix} 1 & & -i \\ & \ddots & \\ & & 1 \end{pmatrix} \\ 1 & & -i & & \\ & & 0 & & \\ & & i & & \\ & & & \ddots & \\ & & & & i \end{pmatrix} \otimes \mathbf{I}_{n \times n} \mathbf{U}_{\text{real}}(t) \end{pmatrix} \quad (86)$$

with the inverse

$$\begin{aligned} \mathbf{U}_{\text{real}}(t) &:= \mathbf{T}^{-T} \mathbf{U}_{\text{cplx}}(t) \\ &= \begin{pmatrix} \begin{pmatrix} 1 & & \\ & \frac{1}{2} & \frac{1}{2} \\ & \ddots & \\ & & \frac{1}{2} \end{pmatrix} \\ \frac{1}{2} & & & & \\ & & \frac{1}{2} & 0 & -\frac{1}{2} \\ & & & \ddots & \\ \frac{1}{2} & & & & \frac{1}{2} \end{pmatrix} \otimes \mathbf{I}_{n \times n} \mathbf{U}_{\text{cplx}}(t). \end{pmatrix} \quad (87)$$

From Section 4.2 we know that the real- and complex-valued Fourier coefficients are then related by

$$\mathbf{X}_{\text{real}} = \mathbf{T} \mathbf{X}_{\text{cplx}} \quad (88)$$

$$\mathbf{X}_{\text{cplx}} = \mathbf{T}^{-1} \mathbf{X}_{\text{real}}. \quad (89)$$

Consequently, the Hill matrices are related by

$$\mathbf{H}_{\text{cplx}} = \mathbf{T}^{-1} \mathbf{H}_{\text{real}} \mathbf{T}. \quad (90)$$

This similarity transformation can also be used to show by straightforward but tedious algebraic calculations that (84) is indeed the correct Hill matrix formulation for $N = 2$.

References

- [1] Y. Colaitis, A. Batailly, Stability analysis of periodic solutions computed for blade-tip/casing contact problems, *J. Sound Vib.* 538 (2022) 117219, <http://dx.doi.org/10.1016/j.jsv.2022.117219>.
- [2] A. Mélot, E. Rigaud, J. Perret-Liaudet, Bifurcation tracking of geared systems with parameter-dependent internal excitation, *Nonlinear Dynam.* 107 (1) (2021) 413–431, <http://dx.doi.org/10.1007/s11071-021-07018-6>.
- [3] V. Fréour, L. Guillot, H. Masuda, S. Usa, E. Tominaga, Y. Tohgi, C. Vergez, B. Cochelin, Numerical continuation of a physical model of brass instruments: Application to trumpet comparisons, *J. Acoust. Soc. Am.* 148 (2) (2020) 748–758, <http://dx.doi.org/10.1121/10.0001603>.
- [4] M. Debeurre, A. Grolet, B. Cochelin, O. Thomas, Finite element computation of nonlinear modes and frequency response of geometrically exact beam structures, *J. Sound Vib.* 548 (2023) 117534, <http://dx.doi.org/10.1016/j.jsv.2022.117534>.
- [5] M. Krack, J. Gross, Harmonic Balance for Nonlinear Vibration Problems, Springer, Cham, 2019, <http://dx.doi.org/10.1007/978-3-030-14023-6>.
- [6] L. Peletan, S. Baguet, M. Torkhani, G. Jacquet-Richardet, A comparison of stability computational methods for periodic solution of nonlinear problems with application to rotordynamics, *Nonlinear Dynam.* 72 (3) (2013) 671–682, <http://dx.doi.org/10.1007/s11071-012-0744-0>.
- [7] J. Zhou, T. Hagiwara, M. Araki, Spectral characteristics and eigenvalues computation of the harmonic state operators in continuous-time periodic systems, *Syst. Control Lett.* 53 (2) (2004) 141–155, <http://dx.doi.org/10.1016/j.sysconle.2004.03.002>.
- [8] J. Wu, L. Hong, J. Jiang, A robust and efficient stability analysis of periodic solutions based on harmonic balance method and Floquet-Hill formulation, *Mech. Syst. Signal Process.* 173 (2022) 109057, <http://dx.doi.org/10.1016/j.ymsp.2022.109057>.
- [9] L. Guillot, A. Lazarus, O. Thomas, C. Vergez, B. Cochelin, A purely frequency based Floquet-Hill formulation for the efficient stability computation of periodic solutions of ordinary differential systems, *J. Comput. Phys.* 416 (2020) 109477, <http://dx.doi.org/10.1016/j.jcp.2020.109477>.
- [10] A. Lazarus, O. Thomas, A harmonic-based method for computing the stability of periodic solutions of dynamical systems, *Comptes Rendus Mécanique* 338 (9) (2010) 510–517, <http://dx.doi.org/10.1016/j.crme.2010.07.020>.
- [11] B. Bentvelsen, A. Lazarus, Modal and stability analysis of structures in periodic elastic states: Application to the Ziegler column, *Nonlinear Dynam.* 91 (2) (2018) 1349–1370, <http://dx.doi.org/10.1007/s11071-017-3949-4>.
- [12] F. Bayer, R.I. Leine, Sorting-free Hill-based stability analysis of periodic solutions through Koopman analysis, *Nonlinear Dynam.* 111 (9) (2023) 8439–8466, <http://dx.doi.org/10.1007/s11071-023-08247-7>.
- [13] F. Bayer, R.I. Leine, Optimal projection in a Koopman-based sorting-free Hill method, in: *Advances in Nonlinear Dynamics*, vol. I, Springer Nature, Switzerland, 2024, pp. 409–419, http://dx.doi.org/10.1007/978-3-031-50631-4_35.
- [14] B. Cochelin, C. Vergez, A high order purely frequency-based harmonic balance formulation for continuation of periodic solutions, *J. Sound Vib.* 324 (1–2) (2009) 243–262, <http://dx.doi.org/10.1016/j.jsv.2009.01.054>.
- [15] L. Guillot, B. Cochelin, C. Vergez, A generic and efficient Taylor series-based continuation method using a quadratic recast of smooth nonlinear systems, *Internat. J. Numer. Methods Engrg.* 119 (4) (2019) 261–280, <http://dx.doi.org/10.1002/nme.6049>.
- [16] L. Guillot, B. Cochelin, C. Vergez, A Taylor series-based continuation method for solutions of dynamical systems, *Nonlinear Dynam.* 98 (4) (2019) 2827–2845, <http://dx.doi.org/10.1007/s11071-019-04989-5>.
- [17] S. Karkar, B. Cochelin, C. Vergez, A. high order, Purely frequency based harmonic balance formulation for continuation of periodic solutions: The case of non-polynomial nonlinearities, *J. Sound Vib.* 332 (4) (2013) 968–977, <http://dx.doi.org/10.1016/j.jsv.2012.09.033>.
- [18] A.H. Nayfeh, B. Balachandran, *Applied Nonlinear Dynamics*, in: *Wiley series in nonlinear science*, Wiley-VCH, Weinheim, 1995.
- [19] J. Kappauf, S. Bäuerle, H. Hetzler, A combined FD-HB approximation method for steady-state vibrations in large dynamical systems with localised nonlinearities, *Comput. Mech.* (2022) <http://dx.doi.org/10.1007/s00466-022-02225-3>.
- [20] L. Woivode, M. Krack, Are Chebyshev-based stability analysis and Urabe's error bound useful features for harmonic balance? *Mech. Syst. Signal Process.* 194 (2023) 110265, <http://dx.doi.org/10.1016/j.ymsp.2023.110265>.
- [21] U.M. Ascher, R.M.M. Mattheij, R.D. Russell, *Numerical Solution of Boundary Value Problems for Ordinary Differential Equations*, Society for Industrial and Applied Mathematics, 1995, <http://dx.doi.org/10.1137/1.9781611971231>.
- [22] T. Detroux, L. Renson, L. Masset, G. Kerschen, The harmonic balance method for bifurcation analysis of large-scale nonlinear mechanical systems, *Comput. Methods Appl. Mech. Engrg.* 296 (2015) 18–38, <http://dx.doi.org/10.1016/j.cma.2015.07.017>.
- [23] G. Kerschen, M. Peeters, J. Golinval, A. Vakakis, Nonlinear normal modes, Part I: A useful framework for the structural dynamicist, *Mech. Syst. Signal Process.* 23 (1) (2009) 170–194, <http://dx.doi.org/10.1016/j.ymsp.2008.04.002>.
- [24] T.M. Cameron, J.H. Griffin, An alternating frequency/time domain method for calculating the steady-state response of nonlinear dynamic systems, *J. Appl. Mech.* 56 (1) (1989) 149–154, <http://dx.doi.org/10.1115/1.3176036>.
- [25] G. Teschl, *Ordinary Differential Equations and Dynamical Systems*, in: *Graduate Studies in Mathematics*, (no. 140) American Mathematical Society, Providence, Rhode Island, 2012.
- [26] C. Chicone, *Ordinary Differential Equations with Applications*, second ed., Springer, New York, 2006, <http://dx.doi.org/10.1007/0-387-35794-7>.
- [27] G. Floquet, Sur les équations différentielles linéaires à coefficients périodiques, 1883, *Annales scientifiques de l' E.N.S.*
- [28] G. Moore, Floquet theory as a computational tool, *SIAM J. Numer. Anal.* 42 (6) (2005) 2522–2568, <http://dx.doi.org/10.1137/s0036142903434175>.
- [29] G.H.V. Golub, C.F.V. Van Loan, *Matrix Computations*, North Oxford Academic, Oxford, 1986.
- [30] A. Mauroy, Y. Susuki, I. Mezić, Introduction to the Koopman operator in dynamical systems and control theory, in: A. Mauroy, Y. Susuki, I. Mezić (Eds.), *The Koopman Operator in Systems and Control*, in: *Concepts, Methodologies and Applications*, Springer, Cham, 2020, pp. 3–33.
- [31] C. Moler, C. Van Loan, Nineteen dubious ways to compute the exponential of a matrix, twenty-five years later, *SIAM Rev.* 45 (1) (2003) 3–49, <http://dx.doi.org/10.1137/S00361445024180>.
- [32] N.J. Higham, The scaling and squaring method for the matrix exponential revisited, *SIAM J. Matrix Anal. Appl.* 26 (4) (2005) 1179–1193, <http://dx.doi.org/10.1137/04061101x>.
- [33] A.H. Al-Mohy, N.J. Higham, A new scaling and squaring algorithm for the matrix exponential, *SIAM J. Matrix Anal. Appl.* 31 (3) (2009) 970–989, <http://dx.doi.org/10.1137/09074721x>.
- [34] J. Ibáñez, J.M. Alonso, P. Alonso-Jordá, E. Defez, J. Sastre, Two Taylor algorithms for computing the action of the matrix exponential on a vector, *Algorithms* 15 (48) (2022) <http://dx.doi.org/10.3390/a15020048>.
- [35] M. Hochbruck, C. Lubich, On Krylov subspace approximations to the matrix exponential operator, *SIAM J. Numer. Anal.* 34 (5) (1997) 1911–1925, <http://dx.doi.org/10.1137/s0036142995280572>.
- [36] D. Lindblad, C. Frey, L. Junge, G. Ashcroft, N. Andersson, Minimizing aliasing in multiple frequency harmonic balance computations, *J. Sci. Comput.* 91 (2) (2022) <http://dx.doi.org/10.1007/s10915-022-01776-0>.
- [37] Z.A. Shami, C. Giraud-Audine, O. Thomas, A nonlinear piezoelectric shunt absorber with a 2:1 internal resonance: Theory, *Mech. Syst. Signal Process.* 170 (2022) 108768, <http://dx.doi.org/10.1016/j.ymsp.2021.108768>.
- [38] G. Gobat, L. Guillot, A. Frangi, B. Cochelin, C. Touzé, Backbone curves, Neimark-Sacker boundaries and appearance of quasi-periodicity in nonlinear oscillators: Application to 1:2 internal resonance and frequency combs in mems, *Meccanica* 56 (8) (2021) 1937–1969, <http://dx.doi.org/10.1007/s11012-021-01351-1>.
- [39] A. Renault, O. Thomas, H. Mahé, Numerical antiresonance continuation of structural systems, *Mech. Syst. Signal Process.* 116 (2019) 963–984, <http://dx.doi.org/10.1016/j.ymsp.2018.07.005>.
- [40] L. Woivode, N.N. Balaji, J. Kappauf, F. Tubita, L. Guillot, C. Vergez, B. Cochelin, A. Grolet, M. Krack, Comparison of two algorithms for harmonic balance and path continuation, *Mech. Syst. Signal Process.* 136 (2020) 106503, <http://dx.doi.org/10.1016/j.ymsp.2019.106503>.
- [41] P. Vigué, C. Vergez, S. Karkar, B. Cochelin, Regularized friction and continuation: Comparison with Coulomb's law, *J. Sound Vib.* 389 (2017) 350–363, <http://dx.doi.org/10.1016/j.jsv.2016.11.002>.
- [42] A. Grolet, A. Vizzaccaro, M. Debeurre, O. Thomas, High order invariant manifold model reduction for systems with non-polynomial non-linearities: geometrically exact finite-element structures and validity limit, *Nonlinear Dynam.* (2024).
- [43] M. Debeurre, A. Grolet, O. Thomas, Quaternion-based finite-element computation of nonlinear modes and frequency responses of geometrically exact beam structures in three dimensions, *Multibody Syst. Dyn.* (2024) <http://dx.doi.org/10.1007/s11044-024-09999-9>.
- [44] L. Guillot, A. Lazarus, O. Thomas, C. Vergez, B. Cochelin, *Manlab 4.0: An Interactive Path-Following and Bifurcation Analysis Software*, Tech. Rep., 2018, URL <http://manlab.lma.cnrs-mrs.fr>.
- [45] A. Bychkov, G. Pogudin, Optimal monomial quadratization for ODE systems, 2021, [arXiv:2103.08013](https://arxiv.org/abs/2103.08013).
- [46] A. Borri, F. Carravetta, P. Palumbo, Quadratized Taylor series methods for ODE numerical integration, *Appl. Math. Comput.* 458 (2023) 128237, <http://dx.doi.org/10.1016/j.amc.2023.128237>.
- [47] F. Carravetta, Global exact quadratization of continuous-time nonlinear control systems, *SIAM J. Control Optim.* 53 (1) (2015) 235–261, <http://dx.doi.org/10.1137/130915418>.
- [48] Y. Cai, G. Pogudin, Dissipative quadratizations of polynomial ODE systems, in: B. Finkbeiner, L. Kovács (Eds.), *Tools and Algorithms for the Construction and Analysis of Systems, TACAS 2024*, in: *Lecture Notes in Computer Science*, Springer Nature, Switzerland, 2024, pp. 323–342, http://dx.doi.org/10.1007/978-3-031-57249-4_16.
- [49] J.G. de Jalón, E. Bayo, *Kinematic and Dynamic Simulation of Multibody Systems*, in: *Mechanical Engineering Series*, Springer, New York, NY, 1994.

- [50] A. Vizzaccaro, A. Opreni, L. Salles, A. Frangi, C. Touzé, High order direct parametrisation of invariant manifolds for model order reduction of finite element structures: Application to large amplitude vibrations and uncovering of a folding point, *Nonlinear Dynam.* 110 (1) (2022) 525–571, <http://dx.doi.org/10.1007/s11071-022-07651-9>.
- [51] C. Touzé, A. Vizzaccaro, O. Thomas, Model order reduction methods for geometrically nonlinear structures: A review of nonlinear techniques, *Nonlinear Dynam.* 105 (2) (2021) 1141–1190, <http://dx.doi.org/10.1007/s11071-021-06693-9>.
- [52] A.W. Naylor, G.R. Sell, *Linear Operator Theory in Engineering and Science*, Holt, Rinehart & Winston, New York, 1971.
- [53] R. Lewandowski, Computational formulation for periodic vibration of geometrically nonlinear structures – part 2: Numerical strategy and examples, *Int. J. Solids Struct.* 34 (15) (1997) 1949–1964, [http://dx.doi.org/10.1016/S0020-7683\(96\)00126-6](http://dx.doi.org/10.1016/S0020-7683(96)00126-6).
- [54] A. Lazarus, O. Thomas, J.-F. Deü, Finite element reduced order models for nonlinear vibrations of piezoelectric layered beams with applications to NEMS, *Finite Elem. Anal. Des.* 49 (1) (2012) 35–51, <http://dx.doi.org/10.1016/j.finela.2011.08.019>.
- [55] A. Vizzaccaro, Y. Shen, L. Salles, Blahoš, C. Touzé, Direct computation of nonlinear mapping via normal form for reduced-order models of finite element nonlinear structures, *Comput. Methods Appl. Mech. Engrg.* 384 (2021) 113957.
- [56] A. Givois, A. Grolet, O. Thomas, J.-F. Deü, On the frequency response computation of geometrically nonlinear flat structures using reduced-order finite element models, *Nonlinear Dynam.* 97 (2) (2019) 1147–1781, <http://dx.doi.org/10.1007/s11071-019-05021-6>.
- [57] M. Géradin, D.J. Rixen, *Mechanical vibrations, Theory and Application to Structural Dynamics*, third ed., Wiley, New York, 2014.
- [58] A. Strauss, J.A. Yorke, On asymptotically autonomous differential equations, *Math. Syst. Theory* 1 (2) (1967) 175–182, <http://dx.doi.org/10.1007/bf01705527>.
- [59] J.F. Dunne, Subharmonic-response computation and stability analysis for a nonlinear oscillator using a split-frequency harmonic balance method, *J. Comput. Nonlinear Dynam.* 1 (3) (2006) 221–229, <http://dx.doi.org/10.1115/1.2198875>.
- [60] S. Narayanan, P. Sekar, A frequency domain based numeric-analytical method for non-linear dynamical systems, *J. Sound Vib.* 211 (3) (1998) 409–424, <http://dx.doi.org/10.1006/jsvi.1997.1319>.
- [61] A. Grolet, F. Thouverez, On a new harmonic selection technique for harmonic balance method, *Mech. Syst. Signal Process.* 30 (2012) 43–60, <http://dx.doi.org/10.1016/j.ymssp.2012.01.024>.
- [62] L. Xie, S. Baguet, B. Prabel, R. Dufour, Bifurcation tracking by harmonic balance method for performance tuning of nonlinear dynamical systems, *Mech. Syst. Signal Process.* 88 (2017) 445–461, <http://dx.doi.org/10.1016/j.ymssp.2016.09.037>.